



## Spin-orbit interactions may relax the rigid conditions leading to flat bands

Nóra Kucska  and Zsolt Gulácsi 

*Department of Theoretical Physics, University of Debrecen, H-4010 Debrecen, Bem ter 18/B, Hungary*



(Received 24 October 2021; revised 17 January 2022; accepted 19 January 2022; published 3 February 2022)

Flat bands are of extreme interest in a broad spectrum of fields since, given their high degeneracy, a small perturbation introduced in the system is able to push the ground state in the direction of an ordered phase of interest. Hence, the flat-band engineering in real materials attracts huge attention. However, manufacturing a flat band represents a difficult task because its appearance in a real system is connected to rigid mathematical conditions relating a part of Hamiltonian parameters. Consequently, whenever a flat band is to be manufactured, these Hamiltonian parameters must be tuned exactly to the values fixed by these rigid mathematical conditions. Here we demonstrate that taking the many-body spin-orbit interaction into account, which can be continuously tuned, e.g., by external electric fields, these rigid mathematical conditions can be substantially relaxed. Consequently, we show that a  $\sim 20\%$ – $30\%$  variation in the Hamiltonian parameters rigidly fixed by the flat-band conditions can also lead to flat bands in the same, or in a bit displaced, position on the energy axis. This percentage can even increase to  $\sim 80\%$  in the presence of an external magnetic field. This study is made for the case of conducting polymers. These systems are relevant not only because they have broad application possibilities, but also because they can be used to present the mathematical background of the flat-band conditions in full generality, in a concise, clear, and understandable manner applicable everywhere in itinerant systems.

DOI: [10.1103/PhysRevB.105.085103](https://doi.org/10.1103/PhysRevB.105.085103)

### I. INTRODUCTION

Flat bands are attracting great interest today given the broad application possibilities of the huge degeneracy they provide. Indeed, flat bands appear in several circumstances as chiral edge-mode broadband topological slow light [1], diffraction-free photonics via collective excited states of atoms in Creutz super-radiance lattices [2], interaction-enhanced group velocity in optical kagome lattices [3], production of topological states in one-dimensional (1D) optical lattices [4], generation of flat bands in non-Hermitian optical lattices [5], realization of tilted Dirac cones from flat bands which lead to intricate transport phenomena [6], engineering flat-band  $PT$ -symmetric metamaterials [7], use of singularities emerging on flat bands [8], artificial flat-band systems [9], and superconducting quantum interference device (SQUID) metamaterials on Lieb lattices [10]. In addition, they are of interest because of the emergence of different ordered phases in flat-band systems such as superconductivity [11], ferromagnetism [12], semimetal magnetic ordering [13], excitonic insulator [14], etc. Flat bands also produce interesting effects as quantized circular photogalvanic effect [15], ordered quantum dot arrays formed by moire excitons [16], emergence of noncontractible loop states [17], etc.

Flat bands occur in several types of materials from which conducting polymers [13,18–22] have broad application possibilities covering thermal conductivity enhancement [23], carrier charge transport [24], heat exchangers and energy storage [25], soft high-performance capacitors [26], switches and commutators [27], sensors [28], high-performance batteries [29], biodegradable plastics [30], light-emitting diodes [31],

organic transistors [32], and even life sciences and medicine [33–35]. This is the reason why in the study of flat-band characteristics, we exemplify the observed properties in the case of conducting polymers.

Flat bands can be effective [20,36,37] or bare (i.e., provided exclusively by  $\hat{H}_{\text{kin}}$ , kinetic energy part of the Hamiltonian). Their main source of difficulties is that they are determined by rigid mathematical conditions connected to the parameters (e.g., hopping matrix elements, coupling constants) of the Hamiltonian ( $\hat{H}$ ). Indeed, deducing the band structure in a lattice, in principle, we obtain from the one-particle part of the Hamiltonian a secular equation of the form

$$Q(\epsilon, \{p_i\}, \{\text{trig}_j(\mathbf{k}\mathbf{x}_\alpha)\}) = 0, \quad (1)$$

where  $\epsilon = E_n(\mathbf{k})$  provides the energy spectrum,  $\{p_i\}$  represents the set of the parameters of the Hamiltonian ( $i = 1, 2, \dots, m_{\text{max}}$ ),  $\mathbf{x}_\alpha$  are the Bravais vectors of the lattice,  $\text{trig}_j(z)$  represent trigonometric functions of  $\sin(nz)$ ,  $\cos(nz)$  type (where  $n$  is an integer) holding in their argument the  $\mathbf{k}$  momentum dependence. The notation  $\{\text{trig}_j(\mathbf{k}\mathbf{x}_\alpha)\}$  represents the set of all trigonometric functions emerging in the secular equation (1). In Eq. (1) all trigonometric contributions  $\text{trig}_j$  emerge in  $Q$  additively, with multiplicative coefficients  $T_j(\{p_i\})$  [i.e., as  $V_j = T_j(\{p_i\})\text{trig}_j(\mathbf{k}\mathbf{x}_\alpha)$ ] which depend on the Hamiltonian parameters  $\{p_i\}$ . Eliminating these coefficients

$$T_j(\{p_i\}) = 0, \quad j = 1, 2, 3, \dots, m \quad (2)$$

the  $\mathbf{k}$  dependence disappears from the secular equation (1), hence, from  $Q = 0$  we find  $\mathbf{k}$  independent  $\epsilon$  values, i.e., flat bands [see for exemplification Eqs. (13)–(15)]. As seen from Eq. (2), when flat bands emerge, interdependencies between

Hamiltonian parameters must be present. If in Eq. (2) one has  $j = 1, 2, \dots, m < m_{\max}$ , these interdependencies rigidly fix the value of  $m$  Hamiltonian parameters. Hence, when a flat band appears, only  $(m_{\max} - m)$  Hamiltonian parameters can be arbitrarily chosen, and  $m$  Hamiltonian parameters remain rigidly fixed [given and determined by the arbitrarily taken  $(m_{\max} - m)$   $\hat{H}$  independent parameters]. One mentions that  $Q$  in Eq. (1) contains additively also a  $V_0 = T_{j=0}$  term which does not contain  $\mathbf{k}$ , and explicitly one has  $Q = \sum_{j=0}^m V_j$  [see also Eq. (25)].

Furthermore, if the  $T_j$  coefficients in  $Q$  also contain the parameter  $\epsilon$ , we can fix the origin of the energy axis to the position of the flat band (i.e.,  $\epsilon = 0$ ), and the deduction of the flat-band conditions can be similarly treated, as presented above in Eqs. (1) and (2). Usually, the flat-band conditions (2) are deduced from a given  $\hat{H}$  describing itinerant systems with independent orbital and spin degrees of freedom. This state of facts is motivated by the observation that the many-body spin-orbit interaction  $\hat{H}_{\text{SO}} = \lambda \sigma \cdot (\nabla V \times \mathbf{k})$  is usually small. Here  $\sigma$  represents the spin of carriers,  $\mathbf{k}$  is their momentum,  $\nabla V$  the potential gradient, while  $\lambda \ll 1$  is the strength of the spin-orbit interaction. When the system is interacting (e.g., the leading term of the Coulomb interaction in a many-body system, the onsite Coulomb repulsion  $U > 0$  is present), the use of  $H_{\text{SO}}$  introduces supplementary complications since because  $\lambda \ll U$  even the perturbative treatment is questionable, hence enforcing special treatment for obtaining exact results [38–40].

Even if the spin-orbit interaction (SOI) is small, its effect is major since it breaks the spin-projection double degeneracy of each band [41], and leads to several interesting effects: stable soliton complexes [42], enhanced transport properties [43], influence of graphene properties [44], coupling of Hofstadter butterfly pairs [45], topological excitations [46], provision of stripe and plane-wave phases [47], able to produce spin-memory loss [48], influence of proximity effects at interfaces [49], leads to anomalous Josephson effect [50] and condensed phases [38]. Furthermore, in several circumstances  $\lambda$  is strongly tunable [51], can be enhanced by Coulomb correlations [52], and can be increased by doping [53], structural conformation (e.g., altering torsion in conjugated polymers) [54], twist of the aromatic rings along the conjugation path [55], and can be even tuned by external electric field [56].

In this paper we show that taking into account  $\hat{H}_{\text{SO}}$  in the system Hamiltonian  $\hat{H}$ , the rigid flat-band conditions in Eq. (2) can be substantially relaxed. This procedure is tempting because the strength of SOI can be continuously tuned by an applied external electric field. Consequently, engineering a flat band in a real system is in fact more easily achievable compared to how it was considered before. As we mentioned previously, we exemplify our results on conducting polymers. Two spin-orbit couplings are considered, one (denoted by  $\lambda$ ) as in base, and another one (denoted by  $\lambda_c$ ) as interbase contribution. In order to obtain more information, also the external magnetic field is considered acting via Peierls phase factors. For the conducting polymer, a pentagon chain is considered (e.g., polyaminotriazole type of chain) since this was one of the first produced conducting polymers.

The remaining part of the paper is constructed as follows: Sec. II presents the studied system, Sec. III deduces the band

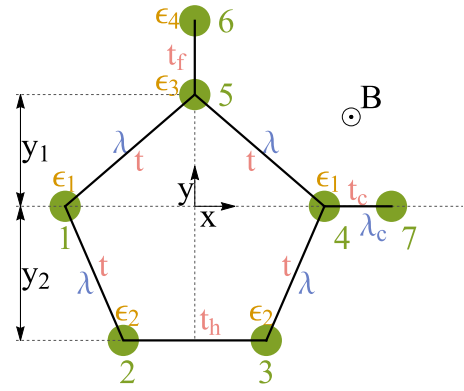


FIG. 1. The pentagonal unit cell, with the nearest-neighbor hopping matrix elements ( $t$ ,  $t_h$ ,  $t_c$ ,  $t_f$ ), the Rashba couplings ( $\lambda$ ,  $\lambda_c$ ), the onsite one-particle potentials ( $\epsilon_1$ ,  $\epsilon_2$ ,  $\epsilon_3$ ,  $\epsilon_4$ ), and the external magnetic field ( $B$ ).

structure, and determines the flat bands, Sec. IV (Sec. V) describes how the mathematically rigid flat-band conditions can be relaxed by spin-orbit interactions maintaining (not maintaining) the position of the flat band, Sec. VI. summarizes the paper, and, finally, Appendixes A–E, containing mathematical details, close the presentation.

## II. THE SYSTEM STUDIED

A schematic plot of the unit cell of the system containing six sites is presented in Fig. 1. The upper antenna in the pentagon chain (as, e.g., in polyaminotriazole, see Fig. 2) is considered simply as the bonds (5,6) on Fig. 1 since this structure is able to describe qualitatively correct its effect in the band structure. The external magnetic field is perpendicular to the plane of the cell. At the level of the Hamiltonian the system is described by

$$\hat{H} = \hat{H}_{\text{kin}} + \hat{H}_{\text{SO}}, \quad (3)$$

where, denoting by  $n = 1, 2, \dots, 6$ , the in-cell position of atoms  $\hat{H}_{\text{kin}}$  is given by

$$\hat{H}_{\text{kin}} = \sum_{i,\sigma} \left[ (t e^{i\phi_{1,5}} \hat{c}_{i,1,\sigma}^\dagger \hat{c}_{i,5,\sigma'} + t e^{i\phi_{2,1}} \hat{c}_{i,2,\sigma}^\dagger \hat{c}_{i,1,\sigma'}) \right]$$

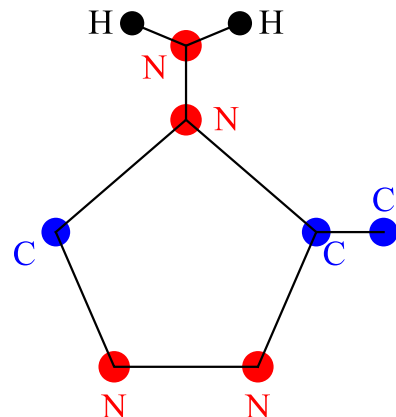


FIG. 2. Schematic plot of the polyaminotriazole cell.

$$\begin{aligned}
 & + t e^{i\phi_{4,3}} \hat{c}_{i,4,\sigma}^\dagger \hat{c}_{i,3,\sigma'} + t e^{i\phi_{5,4}} \hat{c}_{i,5,\sigma}^\dagger \hat{c}_{i,4,\sigma'} \\
 & + t_c e^{i\phi_{7,4}} \hat{c}_{i+a,7,\sigma}^\dagger \hat{c}_{i,4,\sigma'} + t_h e^{i\phi_{3,2}} \hat{c}_{i,3,\sigma}^\dagger \hat{c}_{i,2,\sigma} \\
 & + t_f e^{i\phi_{6,5}} \hat{c}_{i,6,\sigma}^\dagger \hat{c}_{i,5,\sigma} + \text{H.c.}) \\
 & + \left[ \sum_{n=1}^6 \epsilon_n \hat{c}_{i,n,\sigma}^\dagger \hat{c}_{i,n,\sigma} \right]. \quad (4)
 \end{aligned}$$

Here,  $c_{i,n,\sigma}^\dagger$  creates an electron with  $\sigma$  spin projection in the  $n$  position of the cell placed at the site  $i$ ; the  $t, t_h, t_c, t_f$  are nearest-neighbor hopping matrix elements, while  $\epsilon_n$  are the onsite one-particle potentials at the in-cell positions  $n$ . Based on the symmetry of the unit cell, one uses the notations  $\epsilon_1 = \epsilon_{n=1} = \epsilon_{n=4}$ ,  $\epsilon_2 = \epsilon_{n=2} = \epsilon_{n=3}$ ,  $\epsilon_3 = \epsilon_{n=5}$ ,  $\epsilon_4 = \epsilon_{n=6}$ . The Peierls phase factors  $\phi_{n,n'}$  (describing the effect of the external magnetic field on the orbital motion of the carriers) are deduced in Appendix A. Based on the obtained results, one uses the following notations:  $\phi_{3,2} = \phi_1$ ,  $\phi_{4,3} = \phi_{2,1} = \phi_2$ ,  $\phi_{5,4} = \phi_{1,5} = \phi_3$ ,  $\phi_{5,6} = \phi_{7,4} = 0$ .

Concerning  $H_{\text{SO}} = \lambda \sigma \cdot (\nabla V \times \mathbf{k})$ , it introduces spin-flip-type hoppings along the bonds of the system [38]. Since spin-orbit coupling for carbon influences considerably the physical processes in carbon-made materials [57,58], we take into consideration  $H_{\text{SO}}$  on bonds containing carbon atoms. This choice is supported also by the fact that these bonds provide the conjugated (i.e., conducting) nature of the polymer. From these bonds two manifolds can be constructed: in-cell bonds [(1,5);(2,1);(4,3);(5,4); see Fig. 1], and intercell bonds [(7,4) in Fig. 1]. Since the strength of the spin-orbit coupling on intercell bonds can be increased by atom intercalation [59] and the ending atoms on these bonds are different from the ending atoms on in-cell bonds, the SOI coupling on these bonds will be denoted by  $\lambda_c$ , while the in-cell SOI coupling by  $\lambda$ . In these conditions, taking into account Rashba interaction in polymers [56],  $H_{\text{SO}}$  becomes

$$\begin{aligned}
 \hat{H}_{\text{SO}} = & \sum_{i,\sigma} (t_{1,5}^{\sigma,-\sigma} \hat{c}_{i,1,\sigma}^\dagger \hat{c}_{i,5,-\sigma} + t_{2,1}^{\sigma,-\sigma} \hat{c}_{i,2,\sigma}^\dagger \hat{c}_{i,1,-\sigma} \\
 & + t_{4,3}^{\sigma,-\sigma} \hat{c}_{i,4,\sigma}^\dagger \hat{c}_{i,3,-\sigma} + t_{5,4}^{\sigma,-\sigma} \hat{c}_{i,5,\sigma}^\dagger \hat{c}_{i,4,-\sigma} \\
 & + t_c^{\sigma,-\sigma} \hat{c}_{i+a,7,\sigma}^\dagger \hat{c}_{i,4,-\sigma} + \text{H.c.}), \quad (5)
 \end{aligned}$$

where  $\lambda = t_{5,1}^{\uparrow,\downarrow} = t_{1,5}^{\downarrow,\uparrow} = t_{1,2}^{\downarrow,\uparrow} = t_{2,1}^{\uparrow,\downarrow} = t_{3,4}^{\downarrow,\uparrow} = t_{4,3}^{\uparrow,\downarrow} = t_{4,5}^{\downarrow,\uparrow} = t_{5,4}^{\uparrow,\downarrow}$  and  $\lambda_c = t_c^{\uparrow,\downarrow} = t_c^{\downarrow,\uparrow}$ ; furthermore,  $t_{i,j}^{\uparrow,\downarrow} = -t_{j,i}^{\downarrow,\uparrow}$  holds.

As mentioned previously, the strength of  $H_{\text{SO}}$  can be continuously tuned by an applied external electric field [60,61]. One applies the external  $\mathbf{E} = E\bar{k}$  field in the  $z$  direction (per-

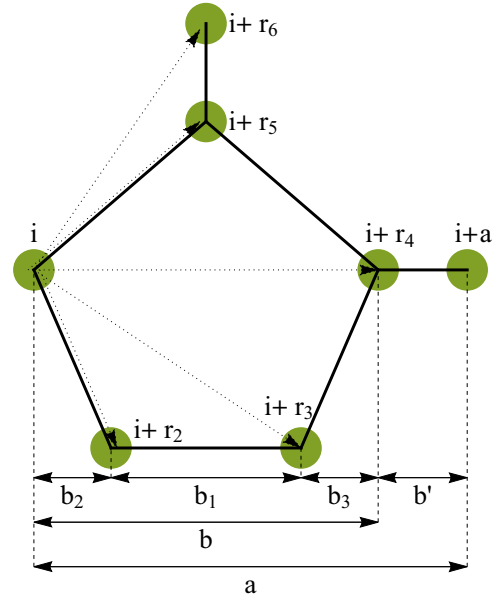


FIG. 3. Notations used for the pentagonal unit cell.

pendicular to the plane of the chain,  $\bar{k}$  being the unit vector in  $z$  direction). Since the carriers move in the  $x$  direction (see Fig. 3), the first quantized Rashba Hamiltonian becomes  $\hat{H}_R = -i\eta\sigma_y k_x$  [56,62] (here  $k_x$  is the momentum along the  $x$  axis, i.e., along the polymer chain), hence the spin is oriented along the  $y$  axis. After this step, if one couples the external magnetic field  $\mathbf{B}$  along the  $z$  axis, since the magnetic induction and the spin vector are perpendicular, the Zeeman term provides zero contribution, and the external magnetic field acts only via the Peierls phase factor. If the source of SOI is exclusively the external electric field,  $\lambda = \lambda_c$ , and the connection of  $\lambda$  to  $E$  is given by [63]

$$\lambda = \bar{K}E, \quad \bar{K} = \frac{|q|\hbar^2}{4m^2c^2} \frac{2\pi}{\lambda_D}, \quad (6)$$

where in the expression of the coefficient  $\bar{K}$ ,  $q$  and  $m$  are the charge and (rest) mass of the carriers,  $\lambda_D$  is their de Broglie wavelength, and  $c$  is the speed of light.

### III. BAND STRUCTURE

First, we transform the  $\hat{H}$  Hamiltonian from Eq. (3) to  $k$  space. The fermionic operators are Fourier transformed via  $\hat{c}_{i,r_n,\sigma} = \frac{1}{\sqrt{N_c}} \sum_k e^{-ik(i+r_n)} \hat{c}_{n,k,\sigma}$ , where  $N_c$  represents the number of unit cells and  $k$  is directed along the  $x$  axis (see Fig. 3). One obtains [see also Eq. (A4)]

$$\begin{aligned}
 \hat{H} = & \sum_k \sum_{\sigma,\sigma'} [t_{1,5}^{\sigma,\sigma'} \hat{c}_{\mathbf{k},1,\sigma}^\dagger \hat{c}_{\mathbf{k},5,\sigma'} e^{i\mathbf{k}(r_1-r_5)} + t_{2,1}^{\sigma,\sigma'} \hat{c}_{\mathbf{k},2,\sigma}^\dagger \hat{c}_{\mathbf{k},1,\sigma'} e^{i\mathbf{k}(r_2-r_1)} + t_{4,3}^{\sigma,\sigma'} \hat{c}_{\mathbf{k},4,\sigma}^\dagger \hat{c}_{\mathbf{k},3,\sigma'} e^{i\mathbf{k}(r_4-r_3)} \\
 & + t_{5,4}^{\sigma,\sigma'} \hat{c}_{\mathbf{k},5,\sigma}^\dagger \hat{c}_{\mathbf{k},4,\sigma'} e^{i\mathbf{k}(r_5-r_4)} + t_c^{\sigma,\sigma'} \hat{c}_{\mathbf{k},1,\sigma}^\dagger \hat{c}_{\mathbf{k},4,\sigma'} e^{i\mathbf{k}(a-r_4)} + t_h \hat{c}_{\mathbf{k},3,\sigma}^\dagger \hat{c}_{\mathbf{k},2,\sigma'} e^{i\mathbf{k}(r_3-r_2)} \\
 & + t_f \hat{c}_{\mathbf{k},6,\sigma}^\dagger \hat{c}_{\mathbf{k},5,\sigma'} e^{i\mathbf{k}(r_6-r_5)} + \text{H.c.}] + \sum_n \epsilon_n \hat{c}_{\mathbf{k},n}^\dagger \hat{c}_{\mathbf{k},n}. \quad (7)
 \end{aligned}$$

Here,  $r_n$  represents the in-cell position of the  $n$ th atoms in the cell, and  $r_1 = 0$  is considered. The terms in the exponents are obtained via (see Fig. 3)

$$\begin{aligned} \mathbf{k}(\mathbf{r}_4 - \mathbf{r}_3) &= \mathbf{k}(\mathbf{r}_2 - \mathbf{r}_1) = kb_2, & \mathbf{k}(\mathbf{r}_6 - \mathbf{r}_5) &= 0, & \mathbf{k}(\mathbf{a} - \mathbf{r}_4) &= kb', \\ \mathbf{k}(\mathbf{r}_3 - \mathbf{r}_2) &= kb_1, & \mathbf{k}(\mathbf{r}_5 - \mathbf{r}_4) &= \mathbf{k}(\mathbf{r}_1 - \mathbf{r}_5) = \frac{kb}{2}. \end{aligned} \quad (8)$$

Using Eq. (8) in (7) one finds

$$\begin{aligned} \hat{H} &= \sum_k \sum_{\sigma, \sigma'} [t_{1,5}^{\sigma, \sigma'} \hat{c}_{\mathbf{k},1,\sigma}^\dagger \hat{c}_{\mathbf{k},5,\sigma'} e^{i\frac{kb}{2}} + t_{2,1}^{\sigma, \sigma'} \hat{c}_{\mathbf{k},2,\sigma}^\dagger \hat{c}_{i,1,\sigma'} e^{ikb_2} + t_{4,3}^{\sigma, \sigma'} \hat{c}_{\mathbf{k},4,\sigma}^\dagger \hat{c}_{\mathbf{k},3,\sigma'} e^{ikb_2} \\ &+ t_{5,4}^{\sigma, \sigma'} \hat{c}_{\mathbf{k},5,\sigma}^\dagger \hat{c}_{\mathbf{k},4,\sigma'} e^{i\frac{kb}{2}} + t_h \hat{c}_{\mathbf{k},3,\sigma}^\dagger \hat{c}_{\mathbf{k},2,\sigma} e^{ikb_1} + t_f \hat{c}_{\mathbf{k},6,\sigma}^\dagger \hat{c}_{\mathbf{k},5,\sigma} + t_c^{\sigma, \sigma'} \hat{c}_{\mathbf{k},1,\sigma}^\dagger \hat{c}_{\mathbf{k},4,\sigma'} e^{ikb'} + \text{H.c.}] + \sum_n \epsilon_n \hat{c}_{\mathbf{k},n}^\dagger \hat{c}_{\mathbf{k},n}. \end{aligned} \quad (9)$$

One observes that  $\hat{H}$  in Eq. (9) can be written as

$$\hat{H} = \sum_k (\hat{c}_{k,1,\uparrow}^\dagger, \dots, \hat{c}_{k,6,\uparrow}^\dagger, \hat{c}_{k,1,\downarrow}^\dagger, \dots, \hat{c}_{k,6,\downarrow}^\dagger) \mathbf{M} \begin{pmatrix} \hat{c}_{k,1,\uparrow} \\ \vdots \\ \hat{c}_{k,6,\uparrow} \\ \hat{c}_{k,1,\downarrow} \\ \vdots \\ \hat{c}_{k,6,\downarrow} \end{pmatrix},$$

where  $\mathbf{M}$ , being a  $12 \times 12$  matrix, can be written in the following form:

$$\mathbf{M} = \begin{pmatrix} \mathbf{M}_1 & \mathbf{M}_2 \\ \mathbf{M}_3 & \mathbf{M}_4 \end{pmatrix}. \quad (10)$$

Here, the  $\mathbf{M}_j$ ,  $j = 1, 2, 3, 4$ , contributions are given as follows:

$$\begin{aligned} \mathbf{M}_1 &= \begin{pmatrix} \epsilon_1 & t e^{-i(kb_2 + \varphi_2)} & 0 & t_c e^{ikb'} & t e^{-i(\frac{kb}{2} - \varphi_3)} & 0 \\ t e^{i(kb_2 + \varphi_2)} & \epsilon_2 & t_h e^{-i(kb_1 + \varphi_1)} & 0 & 0 & 0 \\ 0 & t_h e^{i(kb_1 + \varphi_1)} & \epsilon_2 & t e^{-i(kb_2 + \varphi_2)} & 0 & 0 \\ t_c e^{-ikb'} & 0 & t e^{i(kb_2 + \varphi_2)} & \epsilon_1 & t e^{i(\frac{kb}{2} - \varphi_3)} & 0 \\ t e^{i(\frac{kb}{2} - \varphi_3)} & 0 & 0 & t e^{-i(\frac{kb}{2} - \varphi_3)} & \epsilon_3 & t_f \\ 0 & 0 & 0 & 0 & t_f & \epsilon_4 \end{pmatrix}, \\ \mathbf{M}_2 &= \begin{pmatrix} 0 & -\lambda e^{-i(kb_2 + \varphi_2)} & 0 & \lambda_c e^{ikb'} & -\lambda e^{-i(\frac{kb}{2} - \varphi_3)} & 0 \\ \lambda e^{i(kb_2 + \varphi_2)} & 0 & 0 & 0 & 0 & 0 \\ 0 & 0 & 0 & -\lambda e^{-i(kb_2 + \varphi_2)} & 0 & 0 \\ -\lambda_c e^{-ikb'} & 0 & \lambda e^{i(kb_2 + \varphi_2)} & 0 & \lambda e^{i(\frac{kb}{2} - \varphi_3)} & 0 \\ \lambda e^{i(\frac{kb}{2} - \varphi_3)} & 0 & 0 & -\lambda e^{-i(\frac{kb}{2} - \varphi_3)} & 0 & 0 \\ 0 & 0 & 0 & 0 & 0 & 0 \end{pmatrix}, \\ \mathbf{M}_3 &= \begin{pmatrix} 0 & \lambda e^{-i(kb_2 + \varphi_2)} & 0 & -\lambda_c e^{ikb'} & \lambda e^{-i(\frac{kb}{2} - \varphi_3)} & 0 \\ -\lambda e^{i(kb_2 + \varphi_2)} & 0 & 0 & 0 & 0 & 0 \\ 0 & 0 & 0 & \lambda e^{-i(kb_2 + \varphi_2)} & 0 & 0 \\ \lambda_c e^{-ikb'} & 0 & -\lambda e^{i(kb_2 + \varphi_2)} & 0 & -\lambda e^{i(\frac{kb}{2} - \varphi_3)} & 0 \\ -\lambda e^{i(\frac{kb}{2} - \varphi_3)} & 0 & 0 & \lambda e^{-i(\frac{kb}{2} - \varphi_3)} & 0 & 0 \\ 0 & 0 & 0 & 0 & 0 & 0 \end{pmatrix}, \\ \mathbf{M}_4 &= \begin{pmatrix} \epsilon_1 & t e^{-i(kb_2 + \varphi_2)} & 0 & t_c e^{ikb'} & t e^{-i(\frac{kb}{2} - \varphi_3)} & 0 \\ t e^{i(kb_2 + \varphi_2)} & \epsilon_2 & t_h e^{-i(kb_1 + \varphi_1)} & 0 & 0 & 0 \\ 0 & t_h e^{i(kb_1 + \varphi_1)} & \epsilon_2 & t e^{-i(kb_2 + \varphi_2)} & 0 & 0 \\ t_c e^{-ikb'} & 0 & t e^{i(kb_2 + \varphi_2)} & \epsilon_1 & t e^{i(\frac{kb}{2} - \varphi_3)} & 0 \\ t e^{i(\frac{kb}{2} - \varphi_3)} & 0 & 0 & t e^{-i(\frac{kb}{2} - \varphi_3)} & \epsilon_3 & t_f \\ 0 & 0 & 0 & 0 & t_f & \epsilon_4 \end{pmatrix}. \end{aligned}$$

Now, the band structure can be deduced from the secular equation of the matrix  $\mathbf{M}$ , namely,  $\det(\mathbf{M} - \epsilon \mathbf{I}) = 0$ , where  $\epsilon$  represents the energy eigenvalues, while  $I$  is the  $12 \times 12$  identity matrix. This leads to the following equation (see Appendix B):

$$Q = \det(\mathbf{M} - \epsilon \mathbf{I}) = C(A + iV)(A - iV) = 0, \quad (11)$$

which represents in the present case (1). Here,  $C = A_f^2 \bar{\epsilon}_2^2 \bar{\epsilon}_2^2 \bar{\epsilon}_4^2 \bar{\epsilon}_3^2$ ,  $\bar{\epsilon}_3 = \bar{\epsilon}_3 - \frac{|t_f|^2}{\bar{\epsilon}_4}$ ,  $\bar{\epsilon}_2 = \bar{\epsilon}_2 - \frac{|t_h|^2}{\bar{\epsilon}_2}$ ,  $A_f = \bar{\epsilon}_1 - (t^2 + \lambda^2) \left( \frac{\bar{\epsilon}_4}{\bar{\epsilon}_3 \bar{\epsilon}_4 - t_f^2} + \frac{\bar{\epsilon}_2}{\bar{\epsilon}_2^2 - t_h^2} \right)$ . One has  $\bar{\epsilon}_j = \epsilon_j - \epsilon$  ( $j = 1, 2, 3, 4$ ). The expressions of  $A$  and  $V$  are detailed in Appendix B, and one has

$$\begin{aligned} (A + iV) &= A_f - \frac{1}{A_f} \left[ \left( \bar{t}_c^* e^{i\varphi_k} - \frac{-\lambda^2 + t^2}{\bar{\epsilon}_3} e^{i\varphi} + \frac{-\lambda^2 + t^2}{\bar{\epsilon}_2 \bar{\epsilon}_2} t_h \right) + i \left( \bar{\lambda}_c e^{i\varphi_k} + \frac{2\lambda t}{\bar{\epsilon}_3} e^{i\varphi} - \frac{2\lambda t}{\bar{\epsilon}_2 \bar{\epsilon}_2} t_h \right) \right] \\ &\quad \times \left[ \left( \bar{t}_c e^{-i\varphi_k} - \frac{-\lambda^2 + t^2}{\bar{\epsilon}_3} e^{-i\varphi} + \frac{-\lambda^2 + t^2}{\bar{\epsilon}_2 \bar{\epsilon}_2} t_h \right) - i \left( \bar{\lambda}_c^* e^{-i\varphi_k} + \frac{2\lambda t}{\bar{\epsilon}_3} e^{-i\varphi} - \frac{2\lambda t}{\bar{\epsilon}_2 \bar{\epsilon}_2} t_h \right) \right], \\ (A - iV) &= A_f - \frac{1}{A_f} \left[ \left( \bar{t}_c^* e^{i\varphi_k} - \frac{-\lambda^2 + t^2}{\bar{\epsilon}_3} e^{i\varphi} + \frac{-\lambda^2 + t^2}{\bar{\epsilon}_2 \bar{\epsilon}_2} t_h \right) - i \left( \bar{\lambda}_c e^{i\varphi_k} + \frac{2\lambda t}{\bar{\epsilon}_3} e^{i\varphi} - \frac{2\lambda t}{\bar{\epsilon}_2 \bar{\epsilon}_2} t_h \right) \right] \\ &\quad \times \left[ \left( \bar{t}_c e^{-i\varphi_k} - \frac{-\lambda^2 + t^2}{\bar{\epsilon}_3} e^{-i\varphi} + \frac{-\lambda^2 + t^2}{\bar{\epsilon}_2 \bar{\epsilon}_2} t_h \right) + i \left( \bar{\lambda}_c^* e^{-i\varphi_k} + \frac{2\lambda t}{\bar{\epsilon}_3} e^{-i\varphi} - \frac{2\lambda t}{\bar{\epsilon}_2 \bar{\epsilon}_2} t_h \right) \right], \end{aligned} \quad (12)$$

where  $\bar{t}_c = t_c e^{2i\varphi_3}$ ,  $\bar{\lambda}_c = \lambda_c e^{-2i\varphi_3}$ ,  $\varphi_k = ka + \varphi$ ,  $\varphi = \varphi_1 + 2\varphi_2 + 2\varphi_3$  holds, and one has in Eq. (11) the expression  $Q = CI_+I_- = 0$ ,  $I_{\pm} = A \pm iV$ , which cannot be satisfied by  $C = 0$ .

In what follows one analyzes the  $I_+ = 0$  relation providing  $Q = 0$  (note that the same conclusions are provided by the  $I_- = 0$  relation, see Appendix C). In the present situation, for  $Q = 0$  one has

$$I_+ = (A + iV) = T_0 + T_1 \cos(\varphi_k) + T_2 \sin(\varphi_k) = 0, \quad (13)$$

where

$$\begin{aligned} T_0 &= A_f - \frac{1}{A_f} \left[ (\lambda_c^2 + t_c^2) + (\lambda^2 + t^2)^2 \left( \frac{1}{\bar{\epsilon}_3^2} + \frac{t_h^2}{\bar{\epsilon}_2^2 \bar{\epsilon}_2^2} - \frac{t_h}{\bar{\epsilon}_2 \bar{\epsilon}_2 \bar{\epsilon}_3} 2 \cos(\varphi) \right) \right], \\ T_1 &= \frac{1}{A_f} \left( -\cos(2\varphi_3 + \varphi) \frac{2(2\lambda t \lambda_c + t_c(\lambda^2 - t^2))}{\bar{\epsilon}_3} - \sin(2\varphi_3 + \varphi) \frac{2[-2\lambda t t_c + \lambda_c(\lambda^2 - t^2)]}{\bar{\epsilon}_3} \right. \\ &\quad \left. + \cos(2\varphi_3) \frac{2[2\lambda t \lambda_c + t_c(\lambda^2 - t^2)] t_h}{\bar{\epsilon}_2 \bar{\epsilon}_2} + \sin(2\varphi_3) \frac{2[-2\lambda t t_c + \lambda_c(\lambda^2 - t^2)] t_h}{\bar{\epsilon}_2 \bar{\epsilon}_2} \right), \\ T_2 &= \frac{1}{A_f} \left( \cos(2\varphi_3 + \varphi) \frac{2[-2\lambda t t_c + \lambda_c(\lambda^2 - t^2)]}{\bar{\epsilon}_3} - \sin(2\varphi_3 + \varphi) \frac{2[2\lambda t \lambda_c + t_c(\lambda^2 - t^2)]}{\bar{\epsilon}_3} \right. \\ &\quad \left. - \cos(2\varphi_3) \frac{2[-2\lambda t t_c + \lambda_c(\lambda^2 - t^2)] t_h}{\bar{\epsilon}_2 \bar{\epsilon}_2} - \sin(2\varphi_3) \frac{2[2\lambda t \lambda_c + t_c(\lambda^2 - t^2)] t_h}{\bar{\epsilon}_2 \bar{\epsilon}_2} \right). \end{aligned} \quad (14)$$

The here obtained  $T_j = T_j(p_i)$ ,  $j = 1, 2$ , are the terms present in Eq. (2), and in the present case  $\text{trig}_1(\mathbf{kx}_\alpha) = \cos(\varphi_k)$ ,  $\text{trig}_2(\mathbf{kx}_\alpha) = \sin(\varphi_k)$  holds. The flat-band conditions become [see Eq. (2)]

$$T_1 = 0, \quad T_2 = 0. \quad (15)$$

From Eq. (13) and the flat-band conditions (15) one also has  $T_0 = 0$ . In general, this relation determines the position of the flat band.

#### IV. RELAXING THE RIGID FLAT-BAND CONDITIONS WHILE MAINTAINING THE POSITION OF THE FLAT BAND

##### A. Rigidly fixed flat-band conditions

Let us start with the flat-band conditions (15) in the absence of SOI (i.e.,  $\lambda = \lambda_c = 0$ ) and external magnetic field [i.e.,  $\varphi_i = 0$  at  $i = 1, 2, 3$ , see also Eq. (A3), i.e.,  $\phi = 0$  as well].

In doing this job we fix the origin of the energy axis to the position of the flat band (i.e.,  $\epsilon = 0$ ). From Eq. (15) we find

$$|t_f| = \frac{\sqrt{\epsilon_4 [\epsilon_3 t_h - (\epsilon_2^2 - t_h^2)]}}{\sqrt{t_h}}, \quad (16)$$

while the  $T_0 = 0$  condition, by fixing the flat-band position to the origin, provides

$$|t_c| = \frac{(\epsilon_2 + t_h) [\epsilon_1 (\epsilon_2 - t_h) - t^2]}{\sqrt{(\epsilon_2^2 - t_h^2)^2}}. \quad (17)$$

These results are in agreement with the conditions deduced previously in literature [20]. One notes that the sign of the  $(t_f, t_c)$  hopping amplitudes influences the relative position of the flat band in the band structure of the system. For example, for  $(t_f > 0, t_c > 0)$  the flat band appears as the lowest band in the band structure [for  $N_b$  number of atoms in the base (in our case  $N_b = 6$ ) one has  $N_b$  bands in the band

structure], for ( $t_f < 0$ ,  $t_c < 0$ ) the flat band appears in the upper position of the band structure, etc. From Eqs. (16) and (17) the meaning of rigid flat-band conditions can be clearly exemplified: All Hamiltonian parameters excepting  $t_f$ ,  $t_c$  can be arbitrarily chosen [however, the positivity conditions  $\epsilon_4[\epsilon_3 - (\epsilon_2^2 - t_h^2)/t_h] > 0$ ,  $(\epsilon_2 + t_h)[\epsilon_1 - (\epsilon_2 - t_h) - t^2] > 0$  seen in Eqs. (16) and (17) must be satisfied]. But, the  $t_f$  value is rigidly fixed by Eq. (16). Furthermore, Eq. (17), by fixing the flat-band position to  $\epsilon = 0$ , fixes the  $t_c$  value as well. In order to exemplify (see Set 1 of data in Appendix D), if one takes, e.g.,  $\epsilon_1 = 0.17$ ,  $\epsilon_2 = 0.49$ ,  $\epsilon_3 = 0.22$ ,  $\epsilon_4 = 3.36$ ,  $t_h = 1.5$  (as arbitrarily taken Hamiltonian parameters) for the emergence of the flat band, we rigidly need  $t_f = 2.28941$ , and in order to have  $\epsilon = 0$ , we also need to have “rigidly”  $t_c = 1.1601$ . This rigidity is considered to be the main difficulty in obtaining the flat band in practice. One notes (that it often happens) that at  $\epsilon = 0$ , the rigid conditions relating the Hamiltonian parameters provided by  $T_j = 0$ ,  $j > 1$ , and  $T_0 = 0$  become interdependent.

What we do now is as follows: Maintaining the arbitrarily taken Hamiltonian parameters, we modify  $t_f = t_f^{\text{rfbc}}$  value from the rigid condition (16), and  $t_c = t_c^{\text{rfbc}}$  value provided by Eq. (17) leading to flat band at  $\epsilon = 0$ , where rfbc means “rigid flat-band condition.” By this, the studied band becomes dispersive (details presented in Appendix D). But, we show that now taking into account the SOI spin-orbit coupling, the relaxed  $t_f = t_f^{\text{rfbc}} + \Delta t_f$ ,  $t_c = t_c^{\text{rfbc}} + \Delta t_c$  values are able to provide a flat band again. Consequently, not only  $t_f^{\text{rfbc}}$ ,  $t_c^{\text{rfbc}}$  are able to provide the flat band, but also  $t_f = t_f^{\text{rfbc}} + \Delta t_f$ ,  $t_c = t_c^{\text{rfbc}} + \Delta t_c$  do the same job, hence, the rigid flat-band conditions can be relaxed by SOI. By this, taking into account that  $\lambda$ ,  $\lambda_c$  can be tuned [even continuously, e.g., by an external electric field, see Eq. (6)], the setup of a flat band in practice becomes an easier job. In this section, in this process, by keeping  $\epsilon = 0$ , the flat band which emerges by reflattening (i.e., in the presence of  $\Delta t_f \neq 0$ ;  $\Delta t_c \neq 0$ ;  $\lambda$ ,  $\lambda_c \neq 0$ ) will be placed at the origin of the energy axis again. Hence, here we relax the rigid flat-band conditions but we maintain the position of the flat band at the same time. We do this job first in the absence of the  $B$  external magnetic field.

### B. Relaxing the rigid flat-band conditions by SOI at $B = 0$

At  $B = 0$  and SOI present, based on Eq. (14), the flat-band condition at  $\epsilon = 0$  presented in Eq. (15) becomes

$$\begin{aligned} T_1(B=0) &= -\frac{2}{A_f} \left[ 2\lambda t \lambda_c + t_c (\lambda^2 - t^2) \right] \left( \frac{\epsilon_4}{\epsilon_z} - \frac{t_h}{\epsilon_2^2 - t_h^2} \right) = 0, \\ T_2(B=0) &= -\frac{2}{A_f} \left[ 2\lambda t t_c - \lambda_c (\lambda^2 - t^2) \right] \left( \frac{\epsilon_4}{\epsilon_z} - \frac{t_h}{\epsilon_2^2 - t_h^2} \right) = 0, \end{aligned} \quad (18)$$

while the  $T_0 = 0$  relation maintaining the flat band in the origin provides

$$\begin{aligned} T_0(B=0) &= A_f - \frac{1}{A_f} \left[ (\lambda_c^2 + t_c^2) + (\lambda^2 + t^2)^2 \left( \frac{1}{\epsilon_3^2} + \frac{t_h^2}{\epsilon_2^2 \bar{\epsilon}_2^2} \right) \right. \\ &\quad \left. - 2 \frac{t_h}{\epsilon_2 \bar{\epsilon}_2 \bar{\epsilon}_3} \right] = 0. \end{aligned} \quad (19)$$

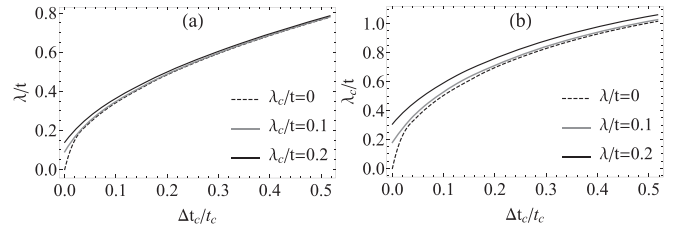


FIG. 4. (a) The  $\lambda$  values necessary to achieve a flat band with different fixed  $\lambda_c$  values, after changing the  $t_c = t_c^{\text{rfbc}}$  value defined by the rigid flat-band conditions by  $\Delta t_c$ . (b) The  $\lambda_c$  values necessary to achieve a flat band with different fixed  $\lambda$  values, after changing the  $t_c = t_c^{\text{rfbc}}$  value defined by the rigid flat-band conditions by  $\Delta t_c$ . For exemplification, we have used the Set 1 of Hamiltonian parameter data from Appendix D.

One notes that the notations  $A_f$ ,  $\bar{\epsilon}_j$ ,  $\bar{\epsilon}_j$ , are given below in Eq. (11). Furthermore, because of  $\epsilon = 0$  one has  $\bar{\epsilon}_j = \epsilon_j$ , and  $\epsilon_z = \epsilon_3 \epsilon_4 - t_f^2$  holds.

In the two lines of Eq. (18) the simultaneous zero value of the two brackets containing  $\lambda$ ,  $\lambda_c$  requires not allowed complex SOI coupling values. Hence, Eq. (18) is satisfied only by  $\epsilon_4(\epsilon_2^2 - t_h^2) = \epsilon_z t_h$ , which leads to the  $t_f = t_f^{\text{rfbc}}$  value presented in Eq. (16). Consequently, if we would like to maintain the position of the flat band (i.e.,  $\epsilon = 0$  has been fixed),  $t_f^{\text{rfbc}}$  cannot be relaxed by SOI couplings. But,  $t_c^{\text{rfbc}}$  [presented in Eq. (17)] can be relaxed by SOI couplings. In order to see this, first one modifies  $t_c$  to the value  $t_c = t_c^{\text{rfbc}} + \Delta t_c$  and makes the flat band dispersive. What is happening explicitly in this step is presented in details in Appendix E, where the dispersive band obtained from the flat band at  $\Delta t_c \neq 0$  and missing SOI is characterized (e.g., see Fig. 12).

In the second step we turn on the SOI which, according to Eq. (19), is able to turn the dispersive band, obtained in the first step, back to a flat band at the same position on the energy scale. What one obtains is exemplified in Fig. 4. The arbitrarily chosen Hamiltonian parameters, together with  $t_f^{\text{rfbc}}$  and  $t_c^{\text{rfbc}}$ , are those used in Appendix D. One observes that even 50% change in  $t_c^{\text{rfbc}}$  can be easily compensated by  $\lambda$  or  $\lambda_c$  in reproducing the flat band in its initial position. One further observes that the in-base SOI ( $\lambda$ ) is more efficient than its interbase ( $\lambda_c$ ) counterpart since smaller  $\lambda$  values are able to compensate the same  $\Delta t_c$  values in reproducing the flat band. As seen, indeed the rigid flat-band condition is substantially relaxed by SOI, at least at the level of  $t_c$ . The price of the reflattened band to remain in the same position is that not all rigidly fixed Hamiltonian parameters can be relaxed (such as  $t_f^{\text{rfbc}}$  in the present case). In such a situation traditional procedures can be combined with SOI in order to achieve the reflattening after the application of the  $\Delta t_c \neq 0$  rigid flat-band condition relaxation. In this case  $\Delta t_f$  can be obtained by changing the side group connected to the pentagon [see Fig. 2, where the side group  $NH_2$  appears in the top (apical) part of the figure]. In the same time with this step, the counterapical (i.e., the N-N bond in Fig. 2) hopping matrix element  $t_h$  must be modified, which can be achieved, e.g., by doping polyaminotriazole with  $ClO_4$  (PAT  $ClO_4$ ), fluorine (PAT F),  $HF_2$  (PAT  $HF_2$ ), etc. What is obtained is exemplified in Fig. 5. We must here underline that higher  $\lambda_c$  values allow

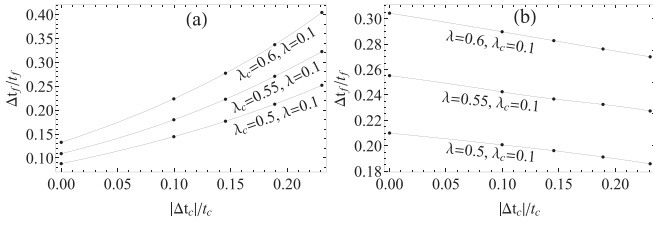


FIG. 5. The  $\lambda$ ,  $\lambda_c$  values necessary to achieve a flat band after changing the  $t_c = t_c^{\text{rfbc}}$  value defined by the rigid flat-band conditions by  $\Delta t_c$ . The changed  $\Delta t_f$  values were obtained by changing the  $t_h$  hopping magnitude, therefore, the value of  $t_h$  is continuously changing along the solid lines, from the original  $t_h$  to  $1.5t_h$ . In case (a) one has  $\lambda = \text{constant}$ , while in the case (b)  $\lambda_c = \text{constant}$  holds. For exemplification, we have used the Set 1 of Hamiltonian parameter data from Appendix D.

higher  $\Delta t_f$  values to be achieved in the attempt to transform the band back to a flat band. Consequently, we mention that by introducing heavy ions on intercell bonds we are able to increase the SOI coupling along the interbase bonds [59], and as seen here, this step would allow to increase the deviation from “rfbc” values in the process of band flattening.

Often, it happens that one has a pentagon polymer chain in which external side groups (apical atoms) are not present, doping is not used, and also heavy-ion introductions on interbase bonds is missing. In this case  $\lambda = \lambda_c = \bar{\lambda}$  values can be tuned by external electric field as specified in Eq. (6). In such conditions, deviations  $\Delta t_c \neq 0$  from  $t_c^{\text{rfbc}}$  can be compensated by  $\bar{\lambda}$  as shown in Fig. 6 in order to create back the flat band at the origin of the energy axis.

### C. Relaxing the rigid flat-band conditions by SOI at $B \neq 0$

When  $B \neq 0$  holds, the flat-band conditions (15) can be written as

$$\frac{1}{A_f}(-K_g v - S_g u) = 0, \quad \frac{1}{A_f}(K_g u - S_g v) = 0, \quad (20)$$

where the following notations have been introduced:

$$K_g = \frac{\cos(4\varphi_3 + \varphi_b)}{\bar{\epsilon}_3} - t_h \frac{\cos(2\varphi_3)}{\bar{\epsilon}_2 \bar{\epsilon}_2},$$

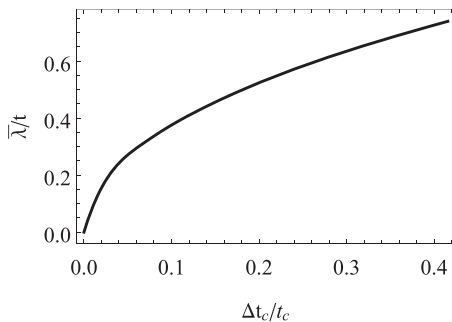


FIG. 6. The  $\bar{\lambda} = \lambda = \lambda_c$  value necessary to compensate the deviation  $\Delta t_c \neq 0$  from  $t_c^{\text{rfbc}}$  in order to recreate the flat band at the origin of the energy axis. For exemplification, we have used the Set 1 of Hamiltonian parameter data from Appendix D.

$$S_g = \frac{\sin(4\varphi_3 + \varphi_b)}{\bar{\epsilon}_3} - t_h \frac{\sin(2\varphi_3)}{\bar{\epsilon}_2 \bar{\epsilon}_2},$$

$$v = 2[2\lambda\lambda_c t + t_c(\lambda^2 - t^2)], \quad u = 2[-2\lambda t t_c + \lambda_c(\lambda^2 - t^2)],$$

$$\varphi = \varphi_b + 2\varphi_3, \quad \varphi_b = \varphi_1 + 2\varphi_2. \quad (21)$$

Since for the Rashba interaction considered here  $\lambda, \lambda_c$  must be real, Eq. (20) allows solutions only for  $K_g = S_g = 0$ , which provide

$$I_c = I_s = I_\varphi, \quad I_\varphi = X_\varphi,$$

$$I_c = \frac{\cos(2\varphi_3)}{\cos(4\varphi_3 + \varphi_b)}, \quad I_s = \frac{\sin(2\varphi_3)}{\sin(4\varphi_3 + \varphi_b)},$$

$$X_\varphi = \frac{\epsilon_4}{t_h} \frac{(\epsilon_2^2 - t_h^2)}{(\epsilon_3 \epsilon_4 - t_f^2)}. \quad (22)$$

For solving Eq. (22) one studies the equality  $I_s = I_c$ . Before starting this job, let us underline that in the limit of zero external magnetic field, this equality gives  $I_\varphi = X_\varphi = 1$  and we reobtain the  $B = 0$  flat-band condition deduced previously in Eq. (16). For  $B \neq 0$ , using  $\sin(\alpha - \beta) = \sin(\alpha)\cos(\beta) - \cos(\alpha)\sin(\beta)$ , the  $I_s = I_c$  relation gives

$$\sin[(4\varphi_3 + \varphi_b) - 2\varphi_3] = \sin(\varphi) = 0, \quad \text{i.e.,} \quad \varphi = \pm n\pi, \quad (23)$$

where  $n$  is an integer number or zero. Hence, at  $I_s = I_c$ , one obtains  $I_s = \sin(2\varphi_3)/\sin(\pm n\pi + 2\varphi_3)$ , consequently,  $I_\varphi = X_\varphi = \pm 1$ , where the upper sign is obtained at  $n = 0$ , while the lower sign is obtained at other  $n$  values. One further observes that when Eq. (23) holds, Eq. (19) remains true, so the first line of Eq. (14) reduces to Eq. (19) when the flat band appears in the presence of the external magnetic field in the same position of the energy axis. Since  $X_\varphi = 1$ , as mentioned above, reproduces the  $B = 0$  results (i.e.,  $\Delta t_c = \Delta t_f = 0$  holds in this case), the  $B \neq 0$  characteristics can be derived from the  $X_\varphi = -1$  relation. Based on the last equality of the second line of Eq. (22), we obtain four different possible deviations  $\Delta t_f$  from the  $t_f^{\text{rfbc}}$  value, which are able to reflatten the band at  $B \neq 0$  in the same position of the energy axis in which was placed the flat band at  $B = 0$ :

$$\Delta t_f = \pm \frac{\sqrt{\epsilon_4[\epsilon_3 t_h - (\epsilon_2^2 - t_h^2)]}}{\sqrt{t_h}} \pm \frac{\sqrt{\epsilon_4[\epsilon_3 t_h + (\epsilon_2^2 - t_h^2)]}}{\sqrt{t_h}}. \quad (24)$$

How  $\Delta t_c$  modifies as a function of the spin-orbit coupling in flattening the band at  $B \neq 0$  (placing the flat band in the same position of the energy axis in which the flat band for  $t_f = t_f^{\text{rfbc}}$ ,  $t_c = t_c^{\text{rfbc}}$  was placed at  $B = 0$ ) is exemplified in Fig. 7. The presented  $|\Delta t_c|/t_c$  results were deduced from the  $T_0$  expression of Eq. (14) in condition of Eq. (23). The  $\bar{\lambda} = \lambda = \lambda_c$  results are similar, and are presented in Fig. 8.

Based on the results presented in this section relating the  $B \neq 0$  case, the following observations can be made: (1) It can be observed that only discrete nonzero external magnetic field values provide reflatting effects [see Eq. (23)]. (2) As shown by Fig. 7 and Eq. (24), huge  $\Delta t_c/t_c$  and  $\Delta t_f/t_f$  values can be achieved at  $B \neq 0$  [allowed by the point (1)] in relaxing the rigid flat-band conditions necessary for obtaining a flat

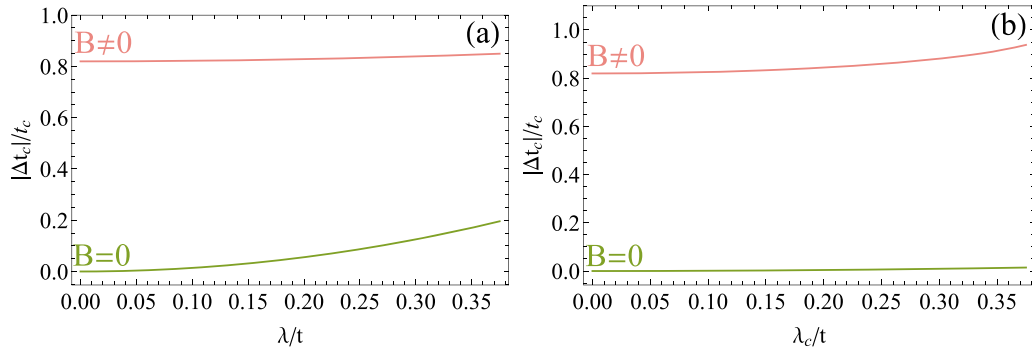


FIG. 7. (a)  $\lambda$  and (b)  $\lambda_c$  spin-orbit coupling values deduced at  $B \neq 0$  (upper) and  $B = 0$  (lower) necessary to compensate the deviation  $\Delta t_c \neq 0$  from  $t_c^{\text{rftbc}}$  in order to recreate the flat band at the origin of the energy axis. For exemplification, we have used the Set 2 of Hamiltonian parameter data from Appendix D.

band in the same position of the energy axis. Figure 7 shows that 80% deviations from  $t_c^{\text{rftbc}}$  can be easily compensated by relatively small spin-orbit interaction values, and based on Eq. (24) it can be checked that 40%–50% deviations from  $t_f^{\text{rftbc}}$  can be achieved in producing a flat band at nonzero  $B$ . (3) The requirement to maintain a fixed flat-band position on the energy axis is relatively restrictive since it does not allow all rigidly fixed flat-band conditions to be continuously relaxed. In the present case, at  $B \neq 0$ , the  $t_f^{\text{rftbc}}$  can be only discretely modified when flat bands are intended to be manufactured. (4) Since the condition in Eq. (23) is connected only to the total flux threading the unit cell, it results that in distorting the unit cell, new aspects in the band flattening via spin-orbit interaction are not encountered.

### V. RELAXING THE RIGID FLAT-BAND CONDITIONS WITHOUT MAINTAINING THE POSITION OF THE FLAT BAND

Let us consider that one has a flat band at  $B = \lambda = \lambda_c = 0$  which is placed in the origin of the energy axis, i.e., at  $\epsilon = e_1 = 0$ . As described previously, for the Hamiltonian parameters, this flat-band emergence requires rigidly fixed flat-band conditions, e.g., in the present case  $t_f = t_f^{\text{rftbc}}$ ,  $t_c = t_c^{\text{rftbc}}$ . Now, we modify  $t_f$  and  $t_c$  with  $\Delta t_f$  and  $\Delta t_c$  relative to  $t_f = t_f^{\text{rftbc}}$

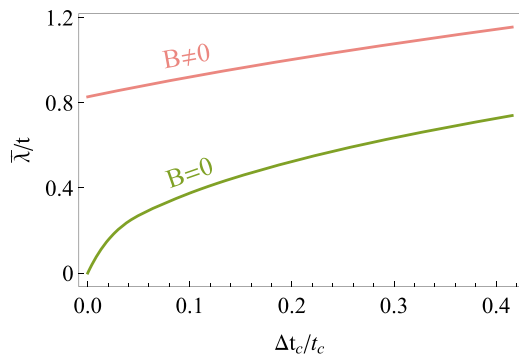


FIG. 8. The  $\bar{\lambda} = \lambda = \lambda_c$  spin-orbit coupling values deduced at  $B \neq 0$  (upper) and  $B = 0$  (lower) necessary to compensate the deviation  $\Delta t_c \neq 0$  from  $t_c^{\text{rftbc}}$  in order to recreate the flat band at the origin of the energy axis. For exemplification, we have used the Set 3 of Hamiltonian parameter data from Appendix D.

and  $t_c = t_c^{\text{rftbc}}$ , the studied flat band becoming dispersive as exemplified in Appendix E. After this step we turn on the SOI such to transform back the dispersive band obtained in the previous step into a flat band placed in the position  $\epsilon = e_2$ . In the preceding Sec. IV, we have analyzed the characteristics of this reflattening process for  $e_1 = e_2 = 0$ , i.e., for the case in which the reflattened band emerges in the same position of the energy axis. Contrary to this, in this section we will analyze the case  $e_1 \neq e_2$ , i.e., the situation in which the starting flat-band position  $e_1$  obtained at  $t_f = t_f^{\text{rftbc}}$ ,  $t_c = t_c^{\text{rftbc}}$ , and  $B = \lambda = \lambda_c = 0$ , will be different from the position  $e_2$  of the flat band obtained via SOI at the end of the process. As it will be seen from the results, this situation allows to considerably relax all rigidly fixed flat-band conditions, hence allows to manufacture flat bands in real systems under easier conditions.

Figures 9 (at  $\Delta t_c/t_c < 0$ ) and 10 (at  $\Delta t_c/t_c > 0$ ) exemplify the obtained results at  $\lambda = 0$ . In these figures, the (a) plots show the  $B = 0$  case, while the (b) plots the  $B \neq 0$  situation. It can be seen that even 20% modification of  $t_c^{\text{rftbc}}$  or  $t_f^{\text{rftbc}}$  can be compensated by the presence of  $\lambda_c$  in reproducing the flat band in a shifted position  $\Delta E$  presented in the inset. It can be observed that all rigidly fixed Hamiltonian parameters can be relaxed in this case. In the presence of the external magnetic field  $B$ , larger  $\Delta t_f/t_f$  deviations can be compensated by smaller  $\lambda_c$  values, which underlines the importance of the consideration of  $B$  in this process. In this case,  $\lambda_c$  can be modified by atom intercalation in the intercell bonds, structural conformation, or twist application [51,53–55].

When one considers the intrinsic  $\lambda$  and  $\lambda_c$  small, and we tune both of them by external electric field, the  $\lambda = \lambda_c = \bar{\lambda}$  case must be considered as presented in Fig. 11, which is plotted at nonzero and constant  $B$ . It can be observed that, e.g., almost 30% positive displacements in  $\Delta t_c/t_c$  and  $\Delta t_f/t_f$  can be compensated by relatively small  $\bar{\lambda}/t$  values of order  $10^{-2}$ .

### VI. FURTHER REMARKS

We would like to add several observations and remarks in what follows.

(a) We approach the presented subject, in a mathematical language, since this allows to show how the flat bands can be detected in general terms in an arbitrary case, how the flat-band conditions can be deduced in a general case, and how a



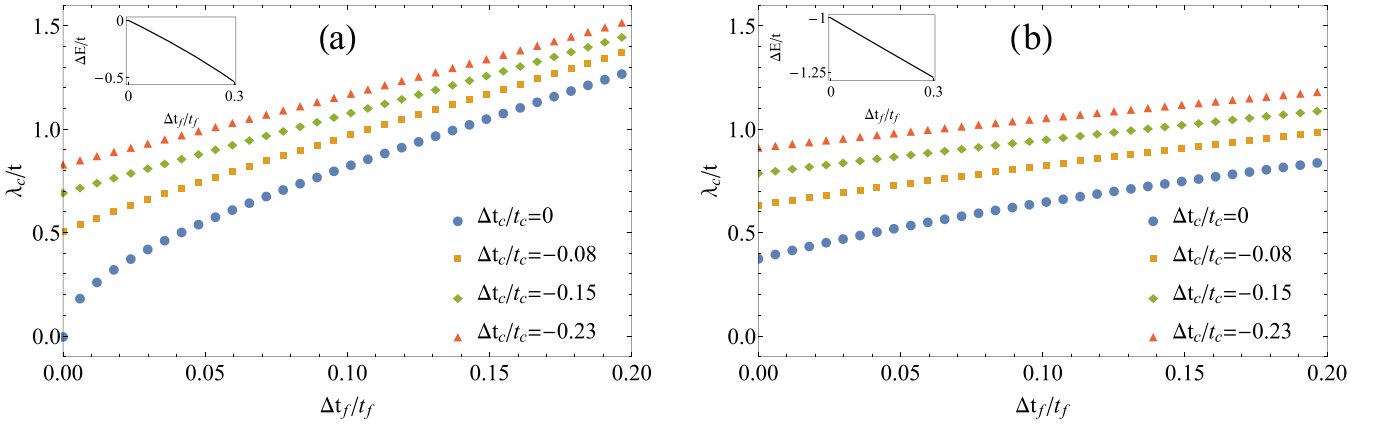


FIG. 9. The  $\lambda_c$  spin-orbit coupling values necessary to compensate at  $\lambda = 0$  the common deviations  $\Delta t_c \neq 0$  and  $\Delta t_f \neq 0$  at (a)  $B = 0$  and (b)  $B \neq 0$ , in order to recreate a flat band placed originally (at  $\lambda = \lambda_c = B = 0$ ) in the origin of the energy axis  $\epsilon = 0$ . The new position of the flat band is at  $\epsilon = \Delta E$ . In this figure  $\Delta t_c/t_c < 0$  holds. For exemplification, we have used the Set 4 of Hamiltonian parameter data from Appendix D.

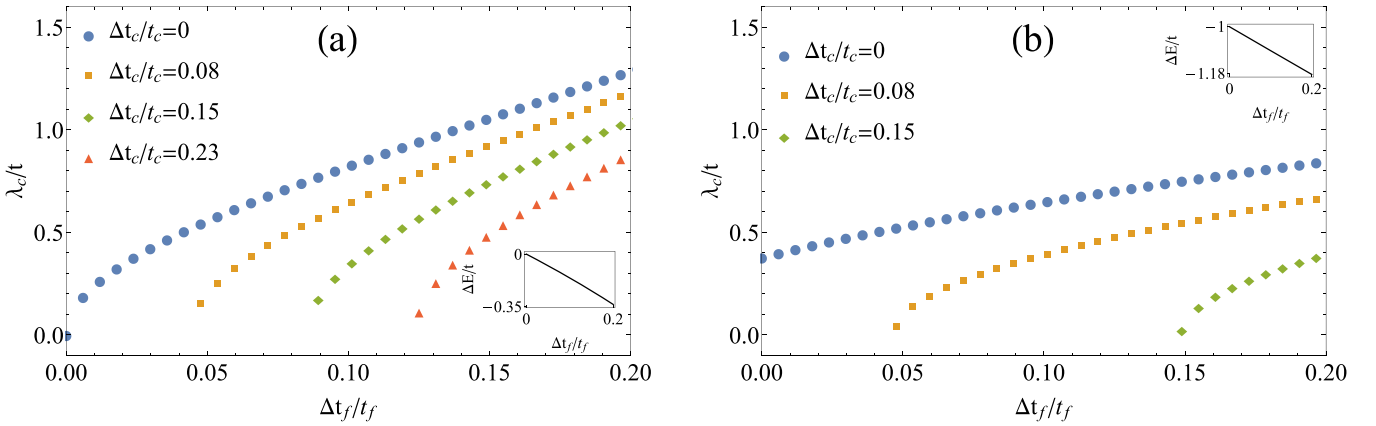


FIG. 10. The  $\lambda_c$  spin-orbit coupling values necessary to compensate at  $\lambda = 0$  the common deviations  $\Delta t_c \neq 0$  and  $\Delta t_f \neq 0$  at (a)  $B = 0$  and (b)  $B \neq 0$  in order to recreate a flat band placed originally (at  $\lambda = \lambda_c = B = 0$ ) in the origin of the energy axis  $\epsilon = 0$ . The new position of the flat band is at  $\epsilon = \Delta E$ . In this figure  $\Delta t_c/t_c > 0$  holds. For exemplification, we have used the Set 4 of Hamiltonian parameter data from Appendix D.

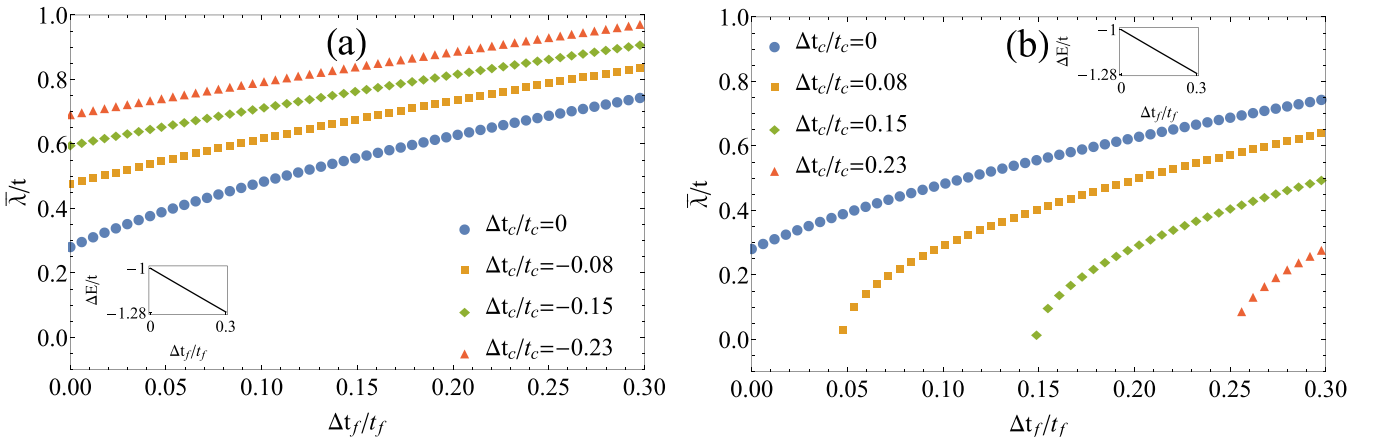


FIG. 11. The  $\lambda_c = \lambda = \bar{\lambda}$  spin-orbit coupling values necessary to compensate the common deviations  $\Delta t_c \neq 0$  and  $\Delta t_f \neq 0$  at  $B \neq 0$  and (a)  $\Delta t_c/t_c < 0$  and (b)  $\Delta t_c/t_c > 0$ , in order to recreate a flat band placed originally (at  $\bar{\lambda} = B = 0$ ) at the origin of the energy axis  $\epsilon = 0$ . The new position of the flat band is at  $\epsilon = \Delta E$ . For exemplification, we have used the Set 4 of Hamiltonian parameter data from Appendix D.

TABLE I. The Sets 1 and 2 of Hamiltonian parameter data.

Set 1						Set 2									
The unrestricted parameters						The parameters calculated from the flat-band conditions		The unrestricted parameters						The parameters calculated from the flat-band conditions	
$\epsilon_1$	$\epsilon_2$	$\epsilon_3$	$\epsilon_4$	$t$	$t_h$	$t_c^{\text{rfbc}}$	$t_f^{\text{rfbc}}$	$\epsilon_1$	$\epsilon_2$	$\epsilon_3$	$\epsilon_4$	$t$	$t_h$	$t_c^{\text{rfbc}}$	$t_f^{\text{rfbc}}$
0.17	0.49	0.22	3.36	1	1.5	1.16	2.29	0.87	1.22	0.82	0.36	1	0.9	2.21	0.14

part of the flat-band conditions enumerated in the literature in fact provide the position of the flat band on the energy scale.

(b) We have used different input parameters in Tables I and II presented in Appendix D in order to underline that our findings, observations, and technical approach to the problem are not related only to one given material, but have an extremely broad application spectrum. The used Hamiltonian parameters are not new, and have not been introduced in this paper: all of them have a broad literature. Consequently, how these parameters affect the band structure is known. For example, in the case of conducting polymers, how the hopping parameters ( $t_i$ ) and onsite one-particle potentials ( $\epsilon_i$ ) influence the band structure is seen, e.g., in [18,20,64,65], etc. How the Peierls phase factors, describing the action of the external magnetic field on the orbital motion of itinerant electrons, act on the band structure is seen, e.g., in [21,66,67], etc. How the many-body spin-orbit interaction acts on the band structure (in most cases the main effect is that it breaks the spin projection double degeneracy of each band) is seen, e.g., in [38,39,68,69], etc. This is why in this paper we concentrate on a single band not satisfying, but being in the absence of, spin-orbit interaction closely placed to the rigid flat-band conditions.

(c) In order to exemplify inside the whole band structure the many-body SOI flattening effect we present Fig. 12, where the polyaminotriazole case is exemplified in zero external magnetic field. The used Hamiltonian parameters are  $t_f/t = 1$  (see Refs. [18,64]), and  $t_h/t = 0.93$ ,  $t_c/t = 1.06$ ,  $\epsilon_1/t = \epsilon_2/t = 0.33$ ,  $\epsilon_3/t = 1.66$ ,  $\epsilon_4/t = 0.8$  (see Ref. [70]). The rigid flat-band conditions require in the absence of external fields and  $\lambda = \lambda_c = 0$  the values  $t_f^{\text{rfbc}} = 1.406$ ,  $t_c^{\text{rfbc}} = 1.996$  (in  $t$  units). As seen,  $\lambda/t = 0.17$  provides  $\Delta t_f/t_f = 0.40$ ,  $\Delta t_c/t_c = 0.88$  relaxation of rigid flat-band conditions. In the presented case, the flat band emerges at the position of the third band ([see Fig. 12(a)]. One notes that, in general, sign

changes in the Hamiltonian parameters change the position of the resulting flat band.

(d) Concerning the contribution of terms not taken into account in the Hamiltonian presented in Eq. (3), the following aspects must be underlined: First, as mentioned previously in the text following Eq. (5), in the used configuration the Zeeman term provides zero contribution because when the external magnetic field  $\mathbf{B}$  is applied, the carrier spin is perpendicular to the magnetic field, hence, the scalar product  $\mathbf{B} \cdot \boldsymbol{\sigma} = 0$  holds. Second, if electric dipole moment  $\mathbf{p}$  is present, it provides a supplementary contribution to the applied external electric field. In the case of the described conducting polymers, the dipole moment vector (if exists) is placed inside the plane  $x$ - $y$  of the polymer. The dipole moment itself originates usually from the inside of the unit cell, being relatively small, as order of magnitude around or below 1 debye [71]. Our analyzed external electric field  $\mathbf{E}$  is perpendicular to the plane of the polymer, so  $\mathbf{E} \cdot \mathbf{p} = 0$ , consequently, the Stark contribution is also missing from the Hamiltonian.

But, it must be mentioned that, in special cases, in order to enhance special applications (e.g., in energy storage or solar cell manufacturing), it is possible to attach to the polymer [72] group of atoms with high dipole moment, even oriented outside of the polymer plane. In such cases, the presented results and findings remain true, but the external electric field is additively renormalized by the electric field created by the dipole moments.

(e) If we concentrate on the question why the flat bands emerge, the answer to this question underlined in this paper is as follows: The band structure is given by the secular equation [ $Q = 0$ , see Eq. (1)] of the one-particle part of the Hamiltonian transformed in the  $k$  space. As explained, always

$$Q = T_0 + \sum_{j=1}^m T_j \text{trig}_j(\mathbf{k}\mathbf{x}_\alpha), \quad (25)$$

TABLE II. The Sets 3 and 4 of Hamiltonian parameter data.

Set 3						Set 4									
The unrestricted parameters						The parameters calculated from the flat-band conditions		The unrestricted parameters						The parameters calculated from the flat-band conditions	
$\epsilon_1$	$\epsilon_2$	$\epsilon_3$	$\epsilon_4$	$t$	$t_h$	$t_c^{\text{rfbc}}$	$t_f^{\text{rfbc}}$	$\epsilon_1$	$\epsilon_2$	$\epsilon_3$	$\epsilon_4$	$t$	$t_h$	$t_c^{\text{rfbc}}$	$t_f^{\text{rfbc}}$
0.11	0.10	0.92	0.86	1	0.85	1.44	1.23	0.65	0.49	1.4	0.86	1	2	1.31	1.68

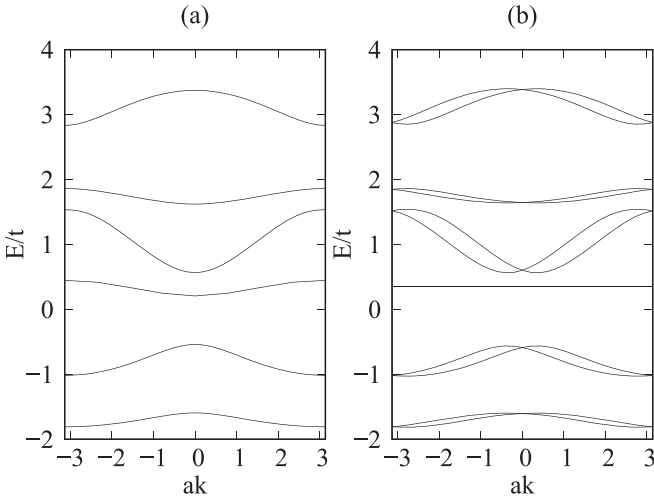


FIG. 12. The many-body spin-orbit interaction effect on the whole band structure: (a) the  $\lambda = \lambda_c = B = 0$  case providing dispersive bands, and (b) at  $B = 0$  the  $\lambda/t = 0.178$  providing a double-degenerate flat band (see Appendix C). For the Hamiltonian parameters, see text.

where  $\mathbf{x}_\alpha$  are the Bravais vectors,  $\mathbf{k}$  the momentum, and the prefactors  $T_0, T_1, \dots, T_m$  depend only on the Hamiltonian parameters  $\{p_i\}$  and the energy  $\epsilon$ . The bands are given by  $\epsilon = E_n(\mathbf{k})$  solutions of the  $Q = 0$  secular equations. Flat bands are obtained always when all  $T_j = 0$  [see Eq. (2)], hence,  $\epsilon$  becomes  $\mathbf{k}$  independent (and the flat-band position will be given by the  $T_0 = 0$  relation). This is the mathematical origin of the flat bands. How do we achieve all the  $T_j = 0$  requirements? We simply tune the Hamiltonian parameters  $\{p_i\}$ . We underline that the here described procedure can be applied always. It also means that flat bands are not the privilege of some special systems since flat bands can be obtained from each system by a proper tuning of the Hamiltonian parameters, a procedure which is effectively often used (see, e.g., Refs. [7,73]). For example, for a simple cubic lattice in a simple tight-binding approximation, from  $Q = 0$  one obtains for the lowest band the relation  $\epsilon - A_0 - A_1[\cos(xk_x) + \cos(yk_y) + \cos(zk_z)] = 0$ , where  $T_0 = \epsilon - A_0$ ,  $T_1 = A_1 \sim t$  holds,  $t$  being the nearest-neighbor hopping integral. The  $T_1 = A_1 = 0$  condition provides a flat band at the position  $\epsilon = A_0$ .

Now, if we ask what it happens physically when all  $T_j = 0$  relations hold, the answer to this question varies from case to case. For example, in the simple cubic lattice case exemplified above,  $A_1 = 0$  occurs when the nearest-neighbor overlap becomes zero (e.g., when we increase the lattice constant at fixed itinerant carrier number, i.e., decrease the carrier concentration), and we reach a low-concentration insulating localized state (e.g., Wigner lattice, since the Coulomb repulsion is always present). The problem becomes complicated also because there are flat bands with itinerant (i.e., nonlocalized) carriers (see, e.g., Ref. [13]). In the situation when carriers are localized in the flat band, often all the  $T_j = 0$  relations are considered related to destructive interference caused by frustration or lattice geometry (see, e.g., Refs. [7,73]). In the conducting polymer case exemplified in this paper, one knows that in the flat band, the one-particle Wannier states are extended over two cells but are localized (see, e.g., Fig. 1 of

Ref. [64]). These Wannier states can be expressed as a linear combination of extended Bloch states. Hence, in explaining the two-cell extension of the Wannier states, the destructive interference argument can be invoked also here.

It is important to stress that independent of how we interpret physically Eq. (2), i.e., all the  $T_j = 0$  relations, the here described procedure in deducing the flat-band emergence always works.

## VII. SUMMARY AND CONCLUSIONS

One knows that in a real system, the emergence of a flat band is connected to rigid mathematical conditions (i.e., flat-band conditions) relating a part of the Hamiltonian parameters (which we denote here by  $\xi_i$ , e.g., in the presented paper,  $\xi_1 = t_c, \xi_2 = t_f$ ). Because of these rigid and restrictive conditions, the engineering of a flat band in a real system is a quite difficult task. Indeed, for this to be possible, the rigidly fixed Hamiltonian parameters must be tuned exactly to the values fixed by the flat-band conditions in order to obtain a flat band in the system. From the other side, given by their high (practically infinitely large) degeneracy, there is a huge need for flat bands in different systems because introducing a small perturbation in such a case, the ground state of such materials can be easily pushed in the direction of several ordered phases of interest in different applications. Because of these reasons, the study of procedures that are able to relax the rigid flat-band conditions is an important task.

Along these lines, in this paper we demonstrate that the many-body spin-orbit interaction (SOI) is able to substantially relax the rigid flat-band conditions, and at the same time can be continuously tuned by external fields. Consequently, taking SOI into account, the flat-band manufacturing in real systems becomes an easier task.

The problem detailed above is analyzed in the case of conducting polymers. Aside from the broad application possibilities of these materials, the motivation of this choice is the fact that the mathematical background of the flat-band conditions can be presented in this case in full generality but in a clear, visible, and understandable manner. One even has the possibility to analyze the action of in-cell ( $\lambda$ ) and intercell ( $\lambda_c$ ) SOI contributions separately. The procedure we use is simple: First, fixing the position of the flat band at the origin of the energy axis  $\epsilon = 0$ , we deduce the flat-band conditions at zero external fields and zero SOI. Then, for a fixed set of Hamiltonian parameters that can be arbitrarily chosen, we deduce the rigidly fixed values of Hamiltonian parameters  $\xi_i = \xi_i^{\text{rfbc}}$ . After this step we destroy the flat band (transforming it into a dispersive band) by modifying  $\xi_i$  from  $\xi_i^{\text{rfbc}}$  to  $\xi_i' = \xi_i^{\text{rfbc}} + \Delta\xi_i$ , and analyze what SOI values transform the dispersive band back into a flat band placed in the position  $\epsilon'$ . In this manner, at the appearance of the flat band, the parameters  $\xi_i$  are no longer rigidly fixed to  $\xi_i^{\text{rfbc}}$ , but take the values  $\xi_i'$ , hence, are relaxed by  $\Delta\xi_i = \xi_i' - \xi_i^{\text{rfbc}}$ .

In the first step we analyze the case  $\epsilon = \epsilon'$ , so the destroyed flat band, after the application of SOI, arrives back in its original position. This situation is usually considered in the literature, and is in fact restrictive since it does not allow to relax all rigidly fixed flat-band conditions. The relaxed parameters, however, calculated as  $\Delta\xi_i/\xi_i$ , can be easily changed by

20%–30% relative to their initial value. The application of an external  $B$  magnetic field increases (at fixed SOI) the possible  $\Delta\xi_i/\xi_i$  values even to 80% (see, e.g., Fig. 7). Comparing to the case mentioned above, we also analyze the case  $\epsilon' \neq \epsilon$  in the second step. In this situation, in fact, mathematically, one of the flat-band conditions is missing, so the rigid flat-band conditions are not so restrictive. In this case, the relative flat-band position displacement on an arbitrary scale  $|\Delta\epsilon/\epsilon|$  is relatively small (i.e., 10%–20%), and contrary to the first case, all rigidly fixed Hamiltonian operator parameters  $\xi_i^{\text{rfbc}}$  can be relaxed by 20%–30% with relatively small SOI coupling values [see, e.g., Fig. 11(b), where even  $\lambda/t < 0.1$ ]. Also in this case, the presence of the external magnetic field enhances the relaxation process of the rigidly fixed Hamiltonian parameter values.

Concerning the question as to how the SOI couplings can be modified and tuned, several possibilities exist. One has discrete tuning possibilities, as for example intercalation of elements with high spin-orbit coupling on bonds connecting cells (e.g., intrachain heavy atoms), hence modifying  $\lambda_c$ . But, more promising possibilities are provided by continuous modification possibilities as, for example, via torsioning, twisting, or application of external electric field. From these, the last possibility seems to be the most attractive [from the data published in the literature (see, e.g., [56]),  $\lambda \sim 0.02$  eV is attained usually by electric fields of order  $E \sim$  kV/cm].

We hope that the presented results will considerably enhance the flat-band engineering of real materials.

## APPENDIX A: PEIERLS PHASE FACTORS

In calculating the  $\varphi_{ji}$  Peierls phase factors, one follows Fig. 1. In the presence of the external magnetic field  $B \neq 0$  they modify the hopping matrix elements according to the relation

$$t_{j \leftarrow i}(B) = t_{j \leftarrow i}(0) e^{i \frac{2\pi}{\phi_0} \int_i^j \vec{A} \cdot \vec{d}l} = t_{j \leftarrow i}(0) e^{i\varphi_{ji}}, \quad (\text{A1})$$

where  $\phi_0 = \frac{hc}{e}$  is the flux quantum. One has  $\varphi_{ji} = \frac{2\pi}{\phi_0} \int_i^j \vec{A} \cdot \vec{d}l$ , and  $t_{j \leftarrow i}(0)$  are the  $B = 0$  hopping matrix elements. Since  $B = \text{rot}(\vec{A})$  holds, and  $B$  points to the  $z$  direction, we use the gauge  $A_x = -By$ ,  $A_y = A_z = 0$ . After this step all exact  $\varphi_{ji}$  Peierls phase factors can be calculated for each bond. One observes that  $\varphi_{56} = 0$  since the scalar product is zero ( $\vec{A} \perp \vec{d}l$ ), and  $\varphi_{47}$  is also 0 because  $y = 0$  holds (see Fig. 1). One obtains

$$\begin{aligned} \varphi_{3 \leftarrow 2} &= \frac{2\pi}{\phi_0} (-By_2), & \varphi_{3 \leftarrow 2} &= \varphi_1, \\ \varphi_{4 \leftarrow 3} &= \frac{2\pi B}{\phi_0} \frac{|y_2|b_2}{2}, & \varphi_{2 \leftarrow 1} &= \varphi_{4 \leftarrow 3} = \varphi_2, \\ \varphi_{5 \leftarrow 4} &= \frac{2\pi B}{\phi_0} \frac{y_1 b}{4}, & \varphi_{5 \leftarrow 4} &= \varphi_{1 \leftarrow 5} = \varphi_3. \end{aligned} \quad (\text{A2})$$

$$\begin{pmatrix} A_f & e^{-ikb}(t_c e^{ika} - W_1) & 0 & e^{-ikb}(\lambda_c e^{ika} - W_2) \\ e^{ikb}(t_c e^{-ika} - W_1^*) & A_f & e^{ikb}(-\lambda_c e^{-ika} + W_2^*) & 0 \\ 0 & e^{-ikb}(-\lambda_c e^{ika} + W_2) & A_f & e^{-ikb}(t_c e^{ika} - W_1) \\ e^{ikb}(\lambda_c e^{-ika} - W_2^*) & 0 & e^{ikb}(t_c e^{-ika} - W_1^*) & A_f \end{pmatrix}, \quad (\text{B1})$$

where  $W_{1f} = (\lambda^2 - t^2)(\frac{1}{\epsilon_2 \epsilon_2} t_h e^{-i\varphi} - \frac{1}{\epsilon_3})$ ,  $W_{2f} = 2\lambda t(\frac{1}{\epsilon_2 \epsilon_2} t_h e^{-i\varphi} - \frac{1}{\epsilon_3})$ .

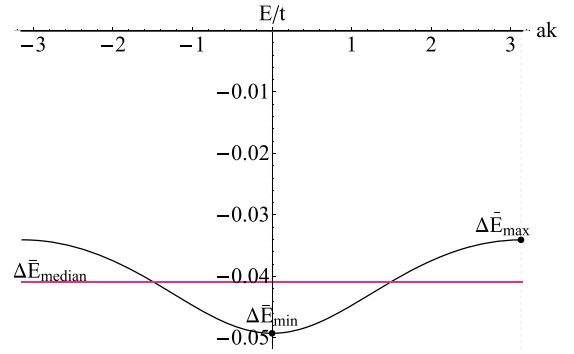


FIG. 13. The flat band originally placed at the origin of the energy axis becomes dispersive under the action of  $\Delta t_c$  at zero SOI couplings. The line in the middle of the dispersive band (at position  $\Delta\bar{E}_{\text{median}}$ ) shows the median of the band, while  $\Delta\bar{E}_{\text{min}}$  and  $\Delta\bar{E}_{\text{max}}$  denote the minimum and maximum positions in the dispersive band relative to the median. The  $\Delta\bar{E}_\alpha$ ,  $\alpha = \text{median, min, max}$ , values are indicated in  $t$  units. For exemplification, we have used the Set 1 of Hamiltonian parameter data from Appendix D.

One further has

$$\varphi = \varphi_1 + 2\varphi_2 + 2\varphi_3 = \frac{2\pi}{\phi_0} \phi, \quad (\text{A3})$$

where  $\phi = BS$  represents the flux trough the unit cell  $S = |y_2|b_1 + 2\frac{|y_2|b_2}{2} + 2\frac{y_1 b}{4}$ .

Taking these results into account, the following hopping terms are present in the Hamiltonian:

$$\begin{aligned} t_{32}^{\uparrow,\uparrow} &= t_h e^{i\varphi_1}, & \varphi_1 &= \frac{2\pi}{\phi_0} (-By_2), \\ t_{21}^{\uparrow,\uparrow} &= t e^{i\varphi_2}, & t_{43}^{\uparrow,\uparrow} &= t e^{i\varphi_2}, & t_{21}^{\uparrow,\downarrow} &= \lambda e^{i\varphi_2}, & t_{43}^{\uparrow,\downarrow} &= \lambda e^{i\varphi_2}, \\ \varphi_2 &= \frac{2\pi}{\phi_0} B \frac{|y_2|b_2}{2}, \\ t_{54}^{\uparrow,\uparrow} &= t e^{i\varphi_3}, & t_{15} &= t e^{i\varphi_3}, & t_{54}^{\uparrow,\downarrow} &= -\lambda e^{i\varphi_3}, & t_{15}^{\uparrow,\downarrow} &= -\lambda e^{i\varphi_3}, \\ \varphi_3 &= \frac{2\pi}{\phi_0} B \frac{y_1 b}{4}, \end{aligned} \quad (\text{A4})$$

while  $t_{i,j}^{\uparrow,\uparrow} = t_{i,j}^{\downarrow,\downarrow}$ ,  $t_{i,j}^{\uparrow,\downarrow} = -t_{i,j}^{\downarrow,\uparrow}$  holds since we have taken only Rashba spin-orbit interactions into account [56].

## APPENDIX B: SECULAR EQUATION

The secular equation (11) in which Eq. (10) has been introduced can be mathematically reduced to the diagonalization of the following  $4 \times 4$  matrix:

Furthermore, the  $A$  and  $V$  expressions present in Eq. (12) are defined as

$$A = A_f - \frac{1}{A_f} (\lambda_c e^{i(\varphi_k - 2\varphi_3)} + 2\lambda t \xi) (\lambda_c e^{-i(\varphi_k - 2\varphi_3)} + 2\lambda t \xi^*) - \frac{1}{A_f} [t_c e^{i(\varphi_k - 2\varphi_3)} - (t^2 - \lambda^2) \xi] [t_c e^{-i(\varphi_k - 2\varphi_3)} - (t^2 - \lambda^2) \xi^*], \quad (\text{B2})$$

where

$$\xi = \left( \frac{\bar{\epsilon}_4}{\bar{\epsilon}_3 \bar{\epsilon}_4 - t_f^2} e^{i\varphi} - \frac{t_h}{\bar{\epsilon}_2^2 - t_h^2} \right) \quad (\text{B3})$$

and

$$V = -\frac{1}{A_f} (\lambda_c e^{i(\varphi_k - 2\varphi_3)} + 2\lambda t \xi) [t_c e^{-i(\varphi_k - 2\varphi_3)} - (t^2 - \lambda^2) \xi^*] - \frac{1}{A_f} (-\lambda_c e^{-i(\varphi_k - 2\varphi_3)} - 2\lambda t \xi^*) [t_c e^{i(\varphi_k - 2\varphi_3)} - (t^2 - \lambda^2) \xi]. \quad (\text{B4})$$

### APPENDIX C: FLAT-BAND CONDITIONS DERIVED FROM THE $(A - iV)$ EXPRESSION

The studied expression can be written as

$$(A - iV) = T_0 + \bar{T}_1 \cos(\varphi_k) + \bar{T}_2 \sin(\varphi_k) = 0, \quad (\text{C1})$$

where  $T_0$  is the same as seen in (14), and  $\bar{T}_1, \bar{T}_2$  are given by

$$\begin{aligned} \bar{T}_1 &= \frac{1}{A_f} \left( -\cos(7\varphi_3) \frac{2[2\lambda t \lambda_c + t_c(\lambda^2 - t^2)]}{\bar{\epsilon}_3} + \sin(7\varphi_3) \frac{2[-2\lambda t t_c + \lambda_c(\lambda^2 - t^2)]}{\bar{\epsilon}_3} \right. \\ &\quad \left. + \cos(2\varphi_3) \frac{2[2\lambda t \lambda_c + t_c(\lambda^2 - t^2)] t_h}{\bar{\epsilon}_2 \bar{\epsilon}_2} - \sin(2\varphi_3) \frac{2[-2\lambda t t_c + \lambda_c(\lambda^2 - t^2)] t_h}{\bar{\epsilon}_2 \bar{\epsilon}_2} \right) = 0, \\ \bar{T}_2 &= \frac{1}{A_f} \left( -\cos(7\varphi_3) \frac{2[-2\lambda t t_c + \lambda_c(\lambda^2 - t^2)]}{\bar{\epsilon}_3} - \sin(7\varphi_3) \frac{2[2\lambda t \lambda_c + t_c(\lambda^2 - t^2)]}{\bar{\epsilon}_3} \right. \\ &\quad \left. + \cos(2\varphi_3) \frac{2[-2\lambda t t_c + \lambda_c(\lambda^2 - t^2)] t_h}{\bar{\epsilon}_2 \bar{\epsilon}_2} + \sin(2\varphi_3) \frac{2[2\lambda t \lambda_c + t_c(\lambda^2 - t^2)] t_h}{\bar{\epsilon}_2 \bar{\epsilon}_2} \right) = 0. \end{aligned} \quad (\text{C2})$$

Using the same notation as in Eq. (20) this expression provides

$$\bar{T}_1 = \frac{1}{A_f} (-K_g v + S_g u) = 0, \quad \bar{T}_2 = \frac{1}{A_f} (-K_g u - S_g v) = 0. \quad (\text{C3})$$

As in the case of Eq. (20), only the solution  $K_g = S_g = 0$  exists, hence, we obtain the solutions derived from the  $(A + iV)$  expression. This is an important result because of the following reason: It is known that usually the many-body spin-orbit interaction breaks the spin-projection double degeneracy of each band [38,41]. But, here one observes that if one creates a flat band using SOI, the flat band will remain double degenerated.

### APPENDIX D: SETS OF HAMILTONIAN PARAMETER DATA

We note that in the Sets 1–4 in Tables I and II all parameters presented are given in  $t$  units, and the rigidly fixed flat-band conditions have been deduced at  $B = \lambda = \lambda_c = 0$ . In the cases of the Sets 2 and 4, when  $B \neq 0$  plots are done, the  $B$  value was deduced from Eq. (22), i.e.,  $I_\varphi = X_\varphi = -1$ . For example, for  $\varphi_b = 3\varphi_3$  (regular pentagon), one has at minimum  $B$  the relation  $\varphi_3 = (1/5)\pi$ . For connection to  $B$ , see also Eq. (A4).

### APPENDIX E: DISPERSIVE BANDS FROM FLAT BANDS

Let us consider that at  $B = \lambda = \lambda_c = 0$  one modifies the  $t_c = t_c^{\text{rbc}}$  rigid flat-band condition value. What happens to the

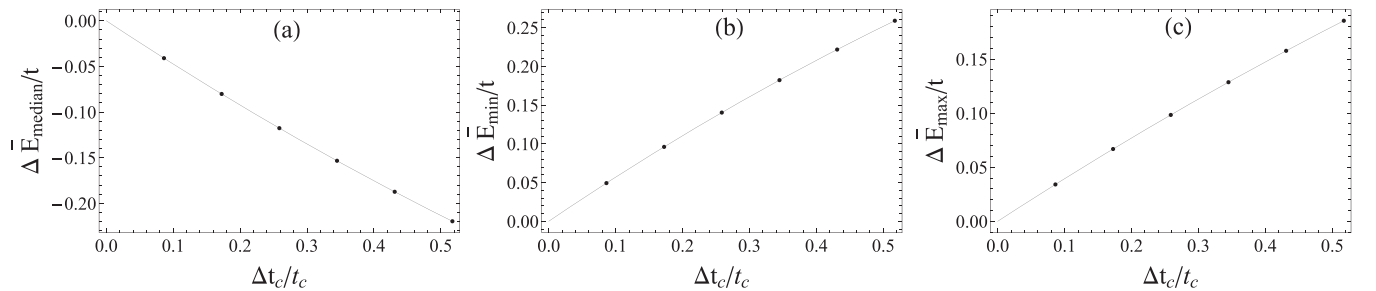


FIG. 14. The different  $\Delta \bar{E}_\alpha$  quantities from Fig. 12 as function of  $\Delta t_c$  normalized to  $t_c = t_c^{\text{rbc}}$ . The presented cases: (a) the median ( $\Delta \bar{E}_{\text{median}}$ ), (b) the maximum ( $\Delta \bar{E}_{\text{max}}$ ), and (c) the minimum ( $\Delta \bar{E}_{\text{min}}$ ). For exemplification, we have used the Set 1 of Hamiltonian parameter data from Appendix D.

band is exemplified in Fig. 13, where 8.62% modification has been taken into account relative to  $t_c^{\text{rfbc}}$ . As seen, the flat band becomes a dispersive band. How  $\Delta\bar{E}_{\text{median}}$ ,  $\Delta\bar{E}_{\text{min}}$ , and  $\Delta\bar{E}_{\text{max}}$  change as function of  $\Delta t_c$  is exemplified in Fig. 14. One notes

that the original flat band placed in the origin of the energy axis was double degenerated relative to the spin projection, and since  $\lambda = \lambda_c = 0$ , this double degeneracy remains valid also in the case of the dispersive band emerging at  $\Delta t_c \neq 0$ .

- 
- [1] L. Yu, H. Xue, and B. Zhang, Topological slow light via coupling chiral edge modes with flat bands, *Appl. Phys. Lett.* **118**, 071102 (2021).
- [2] Y. He, R. Mao, H. Cai, J.-X. Zhang, Y. Li, L. Yuan, S.-Y. Zhu, and D.-W. Wang, Flat-Band Localization in Creutz Superradiance Lattices, *Phys. Rev. Lett.* **126**, 103601 (2021).
- [3] T.-H. Leung, M. N. Schwarz, S.-W. Chang, C. D. Brown, G. Unnikrishnan, and D. Stamper-Kurn, Interaction-Enhanced Group Velocity of Bosons in the Flat Band of an Optical Kagome Lattice, *Phys. Rev. Lett.* **125**, 133001 (2020).
- [4] G. Caceres-Aravena, L. E. F. Foa, and R. A. Vicencio, Topological and flat bands states induced by hybridized interactions in one-dimensional photonic lattices, *Phys. Rev. A* **102**, 023505 (2020).
- [5] S. M. Zhang and L. Jin, Flat band in two-dimensional non-Hermitian optical lattices, *Phys. Rev. A* **100**, 043808 (2019).
- [6] M. Miličević, G. Montambaux, T. Ozawa, I. Sagnes, A. Lemaître, L. Le Gratiet, A. Harouri, J. Bloch, and A. Amo, Type-III and Tilted Dirac Cones Emerging from Flat Bands in Photonic Orbital Graphene, *Phys. Rev. X* **9**, 031010 (2019).
- [7] N. Lazarides and G. P. Tsironis, Compact localized states in engineered flat-band PT metamaterials, *Sci. Rep.* **9**, 4904 (2019).
- [8] J.-W. Rhim and B.-J. Yang, Singular flat bands, *Adv. Phys.: X* **6**, 1901606 (2021).
- [9] D. Leykam, A. Andreanov, and S. Flach, Artificial flat band systems: From lattice models to experiments, *Adv. Phys.: X* **3**, 1473052 (2018).
- [10] N. Lazarides and G. P. Tsironis, SQUID Metamaterials on a Lieb lattice: From flat-band to nonlinear localization, *Phys. Rev. B* **96**, 054305 (2017).
- [11] G. Hu, Q. Ou, G. Si, Y. Wu, J. Wu, Z. Dai, A. Krasnok, Y. Mazar, Q. Zhang, Q. Bao *et al.*, Topological polaritons and photonic magic angles in twisted  $\alpha$ -MoO<sub>3</sub> bilayers, *Nature (London)* **582**, 209 (2020).
- [12] A. Mielke and H. Tasaki, Ferromagnetism in the Hubbard model, *Commun. Math. Phys.* **158**, 341 (1993).
- [13] Z. Gulácsi, A. Kampf, and D. Vollhardt, Route to Ferromagnetism in Organic Polimers, *Phys. Rev. Lett.* **105**, 266403 (2010).
- [14] R. M. Geilhufe and B. Olsthoorn, Identification of strongly interacting organic semimetals, *Phys. Rev. B* **102**, 205134 (2020).
- [15] Z. Ni, B. Xu, M. A. Sanchez-Martinez, Y. Zhang, K. Manna, C. Bernhard, J. W. F. Venderbos, F. de Juan, C. Felser, A. G. Grushin, and L. Wu, Linear and nonlinear optical responses in the chiral multifold semimetal RhSi, *Quantum Mater.* **5**, 96 (2020).
- [16] H. Guo, X. Zhang, and G. Lu, Shedding light on moire excitons: A first-principles perspective, *Sci. Adv.* **6**, eabc5638 (2020).
- [17] W. Yan, H. Zhong, D. Song, Y. Zhang, S. Xia, L. Tang, D. Leykam, and Z. Chen, Flatband line states in photonic super-honeycomb lattices, *Adv. Optical Mater.* **8**, 1902174 (2020).
- [18] Y. Suwa, R. Arita, K. Kuroki, and H. Aoki, Flat-band ferromagnetism in organic polymers designed by a computer simulation, *Phys. Rev. B* **68**, 174419 (2003).
- [19] Z. Gulácsi, A. Kampf, and D. Vollhardt, Exact many-electron ground states on diamond and triangle Hubbard chains, *Prog. Theor. Phys. Suppl.* **176**, 1 (2008).
- [20] Z. Gulácsi, Exact ground states of correlated electrons on pentagon chains, *Int. J. Mod. Phys. B* **27**, 1330009 (2013).
- [21] Z. Gulácsi, A. Kampf, and D. Vollhardt, Exact Many-Electron Ground States on the Diamond Hubbard Chain, *Phys. Rev. Lett.* **99**, 026404 (2007).
- [22] R. Trencsényi, E. Kovács, and Z. Gulácsi, Correlation and confinement induced itinerant ferromagnetism in chain structures, *Philos. Mag.* **89**, 1953 (2009).
- [23] S. Colonna, D. Battagazzore, M. Eleuteri, R. Arrigo, and A. Fina, Properties of graphene-related materials controlling thermal conductivity of their polymer nanocomposites, *Nanomaterials* **10**, 2167 (2020).
- [24] D. Babajanov, H. Matyoqubov, and D. Matrasulov, Charged solitons in branched conducting polymers, *J. Chem. Phys.* **149**, 164908 (2018).
- [25] T. Zhang, X. Wu, and T. Luo, Polymer nanofibers with outstanding thermal conductivity and thermal stability: Fundamental linkage between molecular characteristics and macroscopic thermal properties, *J. Phys. Chem. C* **118**, 21148 (2014).
- [26] J. F. Gu, S. Gorgutsa, and M. Skorobogatiy, Soft capacitor fibers using conductive polymers for electronic textiles, *Smart Mater. Struct.* **19**, 115006 (2010).
- [27] J. Ratzsch, J. Karst, J. Fu, M. Ubl, T. Pohl, F. Sterl, C. Malacrida, M. Wieland, B. Reineke, T. Zentgraf *et al.*, Electrically switchable metasurface for beam steering using PEDOT, *J. Opt.* **22**, 124001 (2020).
- [28] C. Harito, L. Utari, B. R. Putra, B. Yuliarto, S. Purwanto, S. Z. J. Zaidi, D. V. Bavykin, F. Marken, and F. C. Walsh, The development of wearable polymer-based sensors: Perspectives, *J. Electrochem. Soc.* **167**, 037566 (2020).
- [29] P. Sutton, P. Bennington, S. N. Patel, M. Stefik, U. B. Wiesner, P. F. Nealey, U. Steiner, and I. Gunkel, Surface reconstruction limited conductivity in block-copolymer Li battery electrolytes, *Adv. Funct. Mater.* **29**, 1905977 (2019).
- [30] P. Cataldi, P. Steiner, T. Raine, K. Lin, C. Kocabas, R. J. Young, M. Bissett, I. A. Kinloch, and D. G. Papageorgiou, Multi-functional biocomposites based on polyhydroxyalkanoate and graphene/carbon-nanofiber hybrids for electrical and thermal applications, *ACS Appl. Polym. Mater.* **2**, 3525 (2020).
- [31] M. Takada, T. Nagase, T. Kobayashi, and H. Naito, Full characterization of electronic transport properties in working polymer light-emitting diodes via impedance spectroscopy, *J. Appl. Phys.* **125**, 115501 (2019).

- [32] D. A. Bernardis and G. G. Malliaras, Steady-state and transient behavior of organic electrochemical transistors, *Adv. Funct. Mater.* **17**, 3538 (2007).
- [33] Y. Chagnac-Amitai and B. W. Connors, Horizontal spread of synchronized activity in neocortex and its control by GABA-mediated inhibition, *J. Neurophysiol.* **61**, 747 (1989).
- [34] K. A. Ludwig, J. D. Uram, J. Yang, D. C. Martin, and D. R. Kipke, Chronic neural recordings using silicon micro-electrode arrays electrochemically deposited with a poly(3, 4-ethylenedioxythiophene) (PEDOT) film, *J. Neural. Eng.* **3**, 59 (2006).
- [35] G. Schalk, D. J. McFarland, T. Hinterberger, N. Birbaumer, and J. R. Wolpaw, BCI2000: A general-purpose, brain-computer interface (BCI) system, *IEEE Trans. Biomed. Eng.* **51**, 1034 (2004).
- [36] Z. Gulácsi, Interaction-created effective flat bands in conducting polymers, *Eur. Phys. J. B.* **87**, 143 (2014).
- [37] P. Gurin and Z. Gulácsi, Exact solutions for the periodic Anderson model in two dimensions: A non-Fermi-liquid state in the normal phase, *Phys. Rev. B* **64**, 045118 (2001); Erratum: Exact solutions for the periodic Anderson model in two dimensions: A non-Fermi-liquid state in the normal phase [Phys. Rev. B **64**, 045118 (2001)] **65**, 129901(E) (2002).
- [38] N. Kucska and Z. Gulácsi, Exact results relating spin-orbit interactions in two-dimensional strongly correlated systems, *Philos. Mag.* **98**, 1708 (2018).
- [39] N. Kucska and Z. Gulácsi, Itinerant surfaces with spin-orbit couplings, correlations and external magnetic fields: Exact results, *Philos. Mag. Lett.* **99**, 118 (2019).
- [40] N. Kucska and Z. Gulácsi, Nanograin ferromagnets from non-magnetic bulk materials: The case of gold nanoclusters, *Int. J. Mod. Phys. B.* **35**, 2150148 (2021).
- [41] A. Manchon, H. C. Koo, J. Nitta, S. M. Frolov, and R. A. Duine, New perspectives for Rashba spin-orbit coupling, *Nat. Matter.* **14**, 871 (2015).
- [42] Ya. V. Kartashov, E. Ya. Sherman, B. A. Malomed, and V. V. Konotop, Stable two-dimensional soliton complexes in Bose-Einstein condensates with helicoidal spin-orbit coupling, *New J. Phys.* **22**, 103014 (2020).
- [43] Y. Yue, C. A. R. Sá de Melo, and I. B. Spielman, Enhanced transport of spin-orbit coupled Bose gases in disordered potentials, *Phys. Rev. A* **102**, 033325 (2020).
- [44] T. Frank and J. Fabian, Landau levels in spin-orbit coupling proximitized graphene: Bulk states, *Phys. Rev. B* **102**, 165416 (2020).
- [45] Y. Yang, B. Zhen, J. D. Joannopoulos, and M. Soljačić, Non-abelian generalizations of the Hofstadter model: Spin-orbit-coupled Butterfly Pairs, *Light: Sci. Appl.* **9**, 117 (2020).
- [46] H. Yang, Q. Wang, N. Su, and L. Wen, Topological excitations in rotating Bose-Einstein condensates with Rashba-Dresselhaus spin-orbit coupling in a two-dimensional optical lattice, *Eur. Phys. J. Plus* **134**, 589 (2019).
- [47] A. Putra, F. Salces-Cárcoba, Y. Yue, S. Sugawa, and I. B. Spielman, Spatial Coherence of Spin-Orbit-Coupled Bose Gases, *Phys. Rev. Lett.* **124**, 053605 (2020).
- [48] M. Lim and H.-W. Lee, Spin-memory loss induced by bulk spin-orbit coupling at ferromagnet/heavy-metal interfaces, *Appl. Phys. Lett.* **118**, 042408 (2021).
- [49] V. Mishra, Y. Li, F.-C. Zhang, and S. Kirchner, Effects of spin orbit coupling in superconducting proximity devices: Application to CoSi<sub>2</sub>/TiSi<sub>2</sub> heterostructures, *Phys. Rev. B* **103**, 184505 (2021).
- [50] M. Alidoust, C. Shen, and I. Zutic, Cubic spin-orbit coupling and anomalous Josephson effect in planar junctions, *Phys. Rev. B* **103**, L060503 (2021).
- [51] J.-X. Xiong, S. Guan, J.-W. Luo, and S.-S. Li, Emergence of the strong tunable linear Rashba spin-orbit coupling of two-dimensional hole gases in semiconductor quantum, *Phys. Rev. B* **103**, 085309 (2021).
- [52] P. S. Riseborough, S. G. Magalhães, E. J. Calegari, and G. Cao, Enhancement of spin-orbit coupling by strong electronic correlations in transition metals and light actinide compounds, *J. Phys.: Condens. Matter* **32**, 445601 (2020).
- [53] Y. Nakazawa, M. Uchida, S. Nishihaya, M. Ohno, S. Sato, and M. Kawasaki, Enhancement of spin-orbit coupling in Dirac semimetal Cd<sub>3</sub>As<sub>2</sub> films by Sb-doping, *Phys. Rev. B* **103**, 045109 (2021).
- [54] E. Vetter, I. VonWald, S. Yang, L. Yan, S. Koohfar, D. Kumah, Z. G. Yu, W. You, and D. Sun, Tuning of spin-orbit coupling in metal-free conjugated polymers by structural conformation, *Phys. Rev. Mater.* **4**, 085603 (2020).
- [55] D. Beljonne, Z. Shuai, G. Pourtois, and J. L. Bredas, Spin-orbit coupling and intersystem crossing in conjugated polymers: A configuration interaction description, *J. Phys. Chem. A* **105**, 3899 (2001).
- [56] H. Li, M. Y. Zhou, S. Y. Wu, and X. R. Liang, Research of spin-orbit interaction in organic conjugated polymers, *IOP Conf. Ser.: Mater. Sci. Eng.* **213**, 012005 (2017).
- [57] H. F. Rey and H. W. van der Hart, Electron dynamics in the carbon atom induced by spin-orbit interaction, *Phys. Rev. A* **90**, 033402 (2014).
- [58] E. J. G. Santos, A. Ayuela, and D. Sánchez-Portal, Universal magnetic properties of sp<sup>3</sup>-type defects in covalently functionalized graphene, *New J. Phys.* **14**, 043022 (2012).
- [59] D. Sun, K. J. van Schooten, M. Kavand, H. Malissa, C. Zhang, M. Groesbeck, C. Boehme, and Z. V. Vardeny, Inverse spin Hall effect from pulsed spin current in organic semiconductors with tunable spin-orbit coupling, *Nat. Mater.* **15**, 863 (2016).
- [60] J. Nitta, T. Akazaki, and H. Takayanagi, Gate Control of Spin-Orbit Interaction in an Inverted In<sub>0.53</sub>Ga<sub>0.47</sub>As/In<sub>0.52</sub>Al<sub>0.48</sub>As Heterostructure, *Phys. Rev. Lett.* **78**, 1335 (1997).
- [61] G. Engels, J. Lange, Th. Shapers, and H. Luth, Experimental and theoretical approach to spin splitting in modulation-doped In<sub>x</sub>Ga(1-x)As/InP quantum wells for  $B \rightarrow 0$ , *Phys. Rev. B* **55**, R1958 (1997).
- [62] G. Bihlmayer, O. Rader, and R. Winkler, Focus on the Rashba effect, *New J. Phys.* **17**, 050202 (2015).
- [63] H. C. Lee and S.-R. E. Yang, Collective excitation of quantum wires and effect of spin-orbit coupling in the presence of a magnetic field along the wire, *Phys. Rev. B* **72**, 245338 (2005).
- [64] R. Arita, Y. Suwa, K. Kuroki, and H. Aoki, Gate-Induced Band Ferromagnetism in Organic Polymer, *Phys. Rev. Lett.* **88**, 127202 (2002).
- [65] R. Arita, Y. Suwa, K. Kuroki, and H. Aoki, Flat-band ferromagnetism in undoped and doped polyaminotriazole crystal, *Phys. Rev. B* **68**, 140403(R) (2003).
- [66] R. Trencsényi, K. Gulácsi, E. Kovács, and Z. Gulácsi, Exact ground states for polyphenylene type of hexagon chains, *Ann. Phys. (Berlin)* **523**, 741 (2011).

- [67] I. R. Nikolenyi and J. Toth, Magnetic field study of poly (p-phenylenevinylene) derivatives, *J. Magn. Magn. Matter* **517**, 167281 (2021).
- [68] A. Kormanyos, V. Zolyomi, V. I. Falko, and G. Burkard, Tunable Berry curvature and valley and spin-Hall effect in bilayer MoS<sub>2</sub>, *Phys. Rev. B* **98**, 035408 (2018).
- [69] Z. Yu, Y. X. Huang, and S. C. Shen, Spin-orbit splitting of the valence bands in silicon determined by means of high-resolution photoconductive spectroscopy, *Phys. Rev. B* **39**, 6287 (1989).
- [70] H. Mousavi, S. Jalilvand, J. Khodadli, and M. Yousefvand, Tight-binding description of semiconducting conjugated polymers, *Comput. Theor. Chem.* **1199**, 113190 (2021).
- [71] F. Musio and M. C. Ferrara, Low frequency a.c. response of polypyrrole gas sensors, *Sens. Actuators B Chem.* **41**, 97 (1997).
- [72] S. Bonardd, V. Moreno-Serna, G. Kortaberria, D. D. Diaz, A. Leiva, and C. Saldias, Dipolar glass polymers containing polarizable groups as dielectric materials for energy storage applications. A minireview, *Polymers (Basel)* **11**, 317 (2019).
- [73] L. L. Wan, X. Y. Lii, J. H. Gao, and Y. Wu, Hybrid interference induced flat band localization in bipartite optomechanical lattices, *Sci. Rep.* **7**, 15188 (2017).